Oligomeric structure and three-dimensional fold of the HIV gp41 membrane-proximal external region and transmembrane domain in phospholipid bilayers

Citation: Kwon, Byungsu, et al., "Oligomeric structure and three-dimensional fold of the HIV gp41 membrane-proximal external region and transmembrane domain in phospholipid bilayers." Journal of the American Chemical Society 140, 26 (July 2018): p. 8246-59 doi 10.1021/JACS.8B04010 ©2018 Author(s)

As Published: 10.1021/JACS.8B04010

Publisher: American Chemical Society (ACS)

Persistent URL: https://hdl.handle.net/1721.1/125941

Version: Author's final manuscript: final author's manuscript post peer review, without publisher's formatting or copy editing

Published in final edited form as:

J Am Chem Soc. 2018 July 05; 140(26): 8246–8259. doi:10.1021/jacs.8b04010.

Oligomeric Structure and Three-Dimensional Fold of the HIV gp41 MPER and Transmembrane Domain in Phospholipid Bilayers

Byungsu Kwon[1,$], **Myungwoon Lee**[1,$], **Alan J. Waring**[2], and **Mei Hong**[1,*]

[1]Department of Chemistry, Massachusetts Institute of Technology, 170 Albany Street, Cambridge, MA 02139

[2]Department of Medicine, Harbor-UCLA Medical Center, 1000 W. Carson Street, Bldg RB2, Torrance, CA 90502

Abstract

The HIV-1 glycoprotein, gp41, mediates fusion of the virus lipid envelope with the target cell membrane during virus entry into cells. Despite extensive studies of this protein, inconsistent and contradictory structural information abounds in the literature about the C-terminal membrane-interacting region of gp41. This C-terminal region contains the membrane-proximal external region (MPER), which harbors the epitopes for four broadly neutralizing antibodies, and the transmembrane domain (TMD), which anchors the protein to the virus lipid envelope. Due to the difficulty of crystallizing and solubilizing the MPER-TMD, most structural studies of this functionally important domain were carried out using truncated peptides either in the absence of membrane-mimetic solvents or bound to detergents and lipid bicelles. To determine the structural architecture of the MPER-TMD in the native environment of lipid membranes, we have now carried out a solid-state NMR study of the full MPER-TMD segment bound to cholesterol-containing phospholipid bilayers. ^{13}C chemical shifts indicate that the majority of the peptide is α-helical, except for the C-terminus of the TMD, which has moderate β-sheet character. Intermolecular ^{19}F-^{19}F distance measurements of singly fluorinated peptides indicate that the MPER-TMD is trimerized in the virus-envelope mimetic lipid membrane. Intramolecular ^{13}C-^{19}F distance measurements indicate the presence of a turn between the MPER helix and the TMD helix. This is supported by lipid-peptide and water-peptide 2D ^{1}H-^{13}C correlation spectra, which indicate that the MPER binds to the membrane surface whereas the TMD spans the bilayer.

*Corresponding author: Professor Mei Hong, Tel: 617-253-5521, meihong@mit.edu.
$:These authors contributed equally to this work.

Supporting Information Available

Additional tables and NMR spectra include:

1. Sequence alignments of HIV and Ebola viruses' MPER-TMD for MD simulations
2. Further modeling and MD simulation details, including input and output distances and (χ_1, χ_2) torsion angles of fluorinated residues.
3. MPER-TMD peptide mass spectrum, CD data, and lipid mixing data
4. Water-edited 2D ^{13}C-^{13}C correlation spectra
5. 1D and 2D ^{31}P NMR spectra of gp41-containing membranes
6. ^{13}C-^{1}H DIPSHIFT dipolar coupling data
7. ^{19}F CODEX simulation details
8. Alternative trimer models obtained using different starting monomer structures

This material is available free of charge via the Internet at http://pubs.acs.org.

Together, these data indicate that full-length MPER-TMD assembles into a trimeric helix-turn-helix structure in lipid membranes. We propose that the turn between the MPER and TMD may be important for inducing membrane defects in concert with negative-curvature lipid components such as cholesterol and phosphatidylethanolamine, while the surface-bound MPER helix may interact with N-terminal segments of the protein during late stages of membrane fusion.

Graphical Abstract

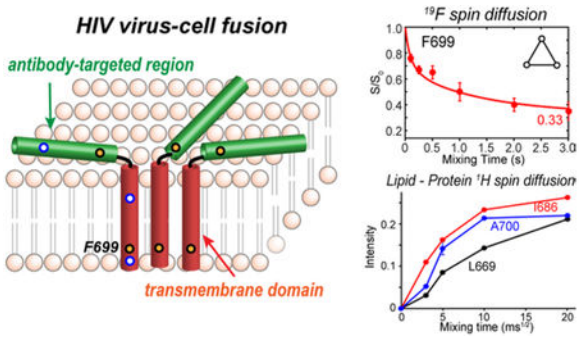

Keywords

solid-state NMR; trimeric structure; virus-cell fusion; ^{19}F spin diffusion; REDOR; membrane curvature induction

Introduction

Human immunodeficiency virus (HIV) enters susceptible cells using the trimeric envelope glycoprotein, Env, which fuses the virus lipid envelope with the cell membrane [1-2]. Proteolytic cleavage of the Env precursor yields two subunits, gp120 and gp41. The former binds to cell-surface receptors and dissociates from the complex, which triggers a cascade of conformational changes in the membrane-interacting subunit, gp41. This cascade starts with refolding of gp41 to expose and insert an N-terminal fusion peptide (FP) into the target cell membrane while the protein remains anchored in the virus envelope through a C-terminal transmembrane domain (TMD) [3]. The extended intermediate then bends onto itself to appose two ectodomain heptad repeats, NHR and CHR (Fig. 1A), to form an antiparallel coiled-coil [4]. This trimer of hairpins, characteristic of the post-fusion structure of class I viral fusion proteins [5-6], brings the two lipid membranes into proximity. The FP and TMD then disorder the cell and virus membranes by mechanisms that are still poorly understood, causing high-curvature membrane intermediates, eventually giving rise to a single merged bilayer. In addition to the FP and TMD, gp41 contains a membrane-proximal external region (MPER) N-terminal to the TMD, which contains highly conserved epitopes for several broadly neutralizing antibodies (bNAbs) [7-10]. A large amount of biochemical and biophysical evidence has shown that both the MPER and TMD are important for HIV entry into cells. For example, Trp-to-Ala mutations in the MPER and deletion of the MPER abrogated virus entry and membrane fusion [11]. Replacement of the gp41 TMD with the vesicular stomatitis virus-G fusion protein TMD severely impacted fusion activity [12].

Truncation of the C-terminus of the TMD in the simian immunodeficiency virus fusion protein reduced fusogenicity [13-14].

Despite the importance of the MPER and TMD for HIV virus-cell fusion, most high-resolution structural studies of gp41 removed all or most of this region due to the difficulty of crystallizing gp41 constructs containing these hydrophobic domains. NMR and EPR studies of gp41 that included part of the MPER-TMD [15-19] have yielded three divergent structural topologies and oligomeric states, as summarized in Fig. 1B-G. The first structural model depicts the MPER as bound to the membrane surface while the TMD spans the bilayer (Fig. 1B). This model is based on NMR and EPR studies of gp41 MPER (residues 662-683) in DPC micelles, which found a distorted helix on the micelle surface [20]. Three polar Asn (N671, N674, and N677) face the aqueous solution, four Trp residues (W666, W670, W672 and W678) are buried in the micelle, and a hinge is present at residues F673-N674 (Fig. 1C). This model is also supported by NMR and EPR studies of the Ebola virus fusion protein MPER-TMD, which found a helix-turn-helix motif, with the MPER lying at the membrane-water interface [21]. However, DEER EPR data showed no intermolecular interactions, indicating that the Ebola MPER-TMD is monomeric in micelles, bicelles and nanodiscs. The second structural model depicts the MPER-TMD as a continuous helix, oriented perpendicular to the membrane plane (Fig. 1D). This model is based on solution NMR studies that included part of the MPER and TMD. For example, a study of gp41 (residues 671-693) found no helical interruption at K683 but a helix kink at G690 in the GxxxG motif of the TMD [22]. Two studies of gp41 (residues 677-716) in DMPC/DHPC bicelles [19, 23] reported an uninterrupted helix from the MPER to the TMD (Fig. 1E). However, these studies differed on the oligomeric state: one study concluded a trimeric coiled coil based on intermolecular cross peaks [19], while the other study found residual dipolar couplings that are inconsistent with C_3 symmetry, and paramagnetic relaxation enhancement and DEER data that indicate an absence of intermolecular contacts [23]. The monomeric helical structure suggests a very tilted orientation for this long helix, to reduce the hydrophobic mismatch between the peptide and the bilayer portion of the bicelle. The third structural model postulates a trimeric MPER and monomeric TMD helices (Fig. 1F), based on studies of a designed MPER peptide (residues 656-683) that is fused with the trimerization domain of bacteriophage T4 fibritin [24]. The structure shows the expected trimeric helices for the N-terminal portion, which splays apart towards the C-terminus of the sequence. This result suggests that bNAbs may interact with individual MPER helices (Fig. 1G) in competition with the membrane surface, and the TMD helices may not be tightly associated in the membrane.

These divergent structural conclusions may arise from the truncated nature of the peptide sequences in most studies, but could also reflect an inherent conformational plasticity of this region of gp41, which may be important for the protein to fold into different structures at different stages of virus-cell fusion. To distinguish these two scenarios, we have synthesized a gp41 peptide (residues 665-704) that spans the entire MPER-TMD region, and investigated the structure of this peptide in phospholipid bilayers using solid-state NMR. The use of lipid bilayers avoids the potential problem of high-curvature micelles and small bicelles to cause non-native protein structures or destabilize protein assembly [25]. We examine the MPER-TMD structure in two membranes, a complex cholesterol-containing membrane that mimics

the HIV lipid envelope composition and a POPE membrane that probes the effect of membrane negative spontaneous curvature on the peptide structure. We address three key aspects of the structure: the three-dimensional fold that describes the relative orientation of the MPER and the TMD, the membrane insertion depths of the MPER and TMD, and the oligomeric state of the entire peptide. We show that in both virus-mimetic membranes and negative-curvature POPE membranes, gp41 MPER-TMD is predominantly α-helical, with the TMD spanning the bilayer while the MPER residing on the membrane surface. Intramolecular distance measurements indicate a turn between the MPER and TMD, while intermolecular distance measurements unequivocally show that the peptide is trimerized. Therefore, this C-terminal domain of gp41 assembles into a trimeric helix-turn-helix in native-like lipid membranes, thus providing structural constraints to mechanistic models of HIV virus-cell fusion.

Materials and Methods

Solid-phase peptide synthesis of site-specific labeled gp41 MPER-TMD

The peptide sequence in this work corresponds to residues 665-704 of gp41 (KWASLW NWFNITNWLW YIKLFIMIVG GLVGLRIVFA VLSI) of HIV-1 clade B HXB2 isolate [26] (UniProtKB/Swiss-Prot: P04578.2) (Table 1).

The peptide was synthesized using Fmoc solid-phase methods on a custom-designed flow peptide synthesizer [27]. 0.05 mmol H-Rink amide ChemMatrix® resin (0.1 g at 0.5 mmol/g loading size) was swelled in the reaction syringe for 5 min in ~5 mL *N,N*-dimethylformamide (DMF) at 70°C. Ten-fold excess (0.5 mmol) of unlabeled amino acid and four-fold excess (0.2 mmol) of isotopically labeled amino acid were singly and doubly coupled, respectively, using a coupling time of 50 s and 70 s. After the final coupling step, the peptide was deprotected and cleaved from the resin by addition of TFA/Phenol/H_2O/TIPS solution (88 : 5 : 5 : 2 by volume) for 3 h. The resin was filtered off, and the crude peptide was precipitated and triturated three times with cold diethyl ether and dissolved in 80% HFIP (1,1,1,3,3,3-Hexafluoro-2-propanol) solution. Crude peptide was purified by reverse-phase HPLC using a Vydac C4 column with a linear gradient of 20-99% channel A over 120 min at a flow rate of 15 mL/min (channel A is 1 : 1 v/v acetonitrile : isopropyl alcohol and channel B is acetonitrile). MALDI-MS analysis verified the mass to be 4818.3 Da for LWIGA and 4835.1 for Da for WLIGF, in agreement with the calculated masses. The combined synthesis and purification yield was ~8%. Three peptide samples with different isotopically labeled positions were prepared (Table 2). ^{13}C, ^{15}N-labeled residues were placed at L669 in MPER, L684, I686, G694, and A700 in the TMD, while fluorinated residues were placed at 5F-W678, 5F-W680, and 4F-F699, where 5F corresponds to the Hζ3 position of Trp and 4F corresponds to the Hζ position of Phe.

Membrane protein sample preparation for SSNMR

The MPER-TMD peptide was reconstituted into the POPE membrane and an HIV virus-mimetic membrane (VMS), which consists of POPC, POPE, POPS, sphingomyelin (SM), and cholesterol at a molar ratio of 30 : 15 : 15 : 10 : 30. The VMS composition differs from the previous virus-mimetic membranes (VM and VM+) [28-29] by including

phosphatidylserine, which is present in the HIV-1 virus envelope at non-negligible levels [30]. Phospholipids were co-dissolved in chloroform and SM was dissolved in a chloroform/methanol mixture. The peptide was dissolved in 2,2,2-trifluoroethanol (TFE) and mixed with the lipid solution. The solvents were removed under nitrogen gas, then the samples were dried under vacuum overnight. The dried powder was resuspended in pH 7.5 HEPES buffer (10 mM HEPES-NaOH, 1 mM EDTA, 0.1 mM NaN_3) and dialyzed against pH 7.5 HEPES buffer for a day with two buffer changes to remove salt and residual TFA and TFE. The vesicle solutions were spun at 40,000 rpm using a Beckman SW60Ti rotor at 4 °C for 4 hours to obtain wet membrane pellets, which were allowed to equilibrate in a desiccator to ~40 wt% water by mass. The samples were then spun into magic-angle-spinning (MAS) rotors through a pipette tip. Most samples in this study have a peptide : lipid (P/L) mole ratio of 1 : 15. For the 4F-F699 labeled peptide reconstituted into the POPE membrane, we prepared two samples at P/L ratios of 1 : 15 and 1 : 45, to investigate whether the oligomeric state of the MPER-TMD is sensitive to the peptide concentration in the range studied here.

Lipid mixing assays

To verify the fusion activity of the MPER-TMD peptide, we conducted lipid mixing assays on POPC/POPG (4:1) vesicles [31]. Two solutions of large unilamellar vesicles (LUVs), with and without fluorescent dyes, were prepared. The unlabeled POPC/POPG LUVs were prepared in 10 mM HEPES buffer at pH 7.5 by 10-12 cycles of freeze-thaw between liquid nitrogen temperature and 35°C, followed by 15-20 cycles of extrusion through 100 nm polycarbonate membranes (Whatman). The fluorescently labeled vesicles differ by containing 2 mol% NBD-PE (1,2-dipalmitoyl-*sn*-glycero-3-phospho-ethanolamine-N-(7-nitro-2-1,3-benzoxadiazol-4-yl)) and 2 mol% of the quenching lipid Rh-PE (1,2-dipalmitoyl-*sn*-glycero-3-phosphoethanolamine-N-(lissamine rhodamine B sulfonyl)). The unlabeled and labeled vesicles were mixed at a 9 : 1 mole ratio and have a total lipid concentration of 75 μM. Then the MPER-TMD peptide was added from a formic acid solution to reach a peptide: lipid mole ratio of 1 : 20. If MPER-TMD causes mixing of the labeled and unlabeled vesicles, then the distances between NBD-PE and Rh-PE will increase, thus dequenching the fluorescence intensity. A HORIBA Fluoromax-P fluorimeter was used to measure fluorescence intensities at an excitation wavelength of 465 nm and an emission wavelength of 530 nm, with a bandwidth of 4 nm. The measurement was carried out at 21°C, under continuous stirring in 2 ml LUVs, with a 1 s time increment.

We designate the initial fluorescence intensity before peptide addition as F_0 and peptide addition as F_f. The maximum fluorescence intensity (F_{max}) is taken as the intensity when 20 μL of 10% Triton X-100 was added to 2 ml of lipid vesicle solution. The percent lipid mixing was calculated using the equation % lipid mixing $=[(F_f - F_0)/(F_{max} - F_0)]\cdot 100$. To test whether the formic acid itself causes lipid mixing, we conducted a control experiment where 5 μL of peptide-free formic acid was added to the lipid vesicle solution. We found that 5 μL formic acid caused only ~5% lipid mixing, compared to 7.2 μL of peptide-containing solution, which induced 75% lipid mixing. Thus the MPER-TMD peptide is chiefly responsible for the observed lipid mixing.

Circular dichroism experiments

Circular dichroism (CD) spectra were measured on an AVIV 202 spectrometer using a 1 mm path-length quartz cuvette to evaluate the secondary structure of the MPER-TMD. The peptide was dissolved in three solutions: TFE, POPC/POPG (4 : 1) membrane, and DOPC/DOPE (2:1) membrane. The membrane samples used a P/L ratio of 1 : 20. 0.05 - 0.10 mg of peptide was dissolved in 0.5 ml vesicle solution and TFE. Control spectra of peptide-free solutions were subtracted from the spectra of peptide-containing samples.

Solid-state NMR experiments

Solid-state NMR spectra were measured on Bruker 400 MHz (9.4 Tesla), 600 MHz (14.1 Tesla), and 800 MHz (18.8 Tesla) spectrometers using 4 mm and 3.2 mm MAS probes. ^{13}C chemical shifts are reported on the TMS scale using the 38.48-ppm CH_2 signal of adamantane and the 14.0-ppm Met Cε signal of the tripeptide N-formyl-Met-Leu-Phe-OH (f-MLF) as indirect standards. ^{31}P chemical shifts were referenced to the 2.73-ppm ^{31}P signal of hydroxyapatite on the phosphoric acid scale. ^{19}F chemical shift was referenced to the −122 ppm ^{19}F signal of Teflon on the $CFCl_3$ scale.

2D ^{13}C-^{13}C DARR correlation spectra [32-33] with a mixing time of 100 ms were measured at 263 K to assign ^{13}C chemical shifts. To determine the depth of insertion of the peptide in lipid bilayers, we conducted a 2D ^{1}H-^{13}C correlation experiment in which a ^{1}H T_2 filter of 0.8 ms was applied to suppress the protein ^{1}H magnetization while retaining water and lipid ^{1}H magnetization [34-35]. After ^{1}H chemical shift evolution, a ^{1}H spin diffusion mixing period of 9 – 400 ms was used to transfer ^{1}H magnetization to the protein and detected through ^{13}C after cross polarization [34]. The experiments were conducted on the LWIGA-labeled peptide in POPE membranes at 303 K under 9 kHz MAS. Cross peak intensities are plotted as a function of the square root of the spin diffusion mixing time, since the solution to the diffusion equation in a two-phase system has an inherent $\sqrt{t}$ dependence [35-36].

To probe the water accessibility of different residues in detail, we measured water-edited 2D ^{13}C-^{13}C correlation spectra at 263 – 273 K under MAS frequencies of 9 kHz and 10.5 kHz [35, 37-39]. At this temperature, with ^{1}H T_2 filters of 0.6 ms to 0.8 ms, the lipid and protein ^{1}H magnetization is largely suppressed, leaving water as the only ^{1}H polarization source. This is followed by a ^{1}H mixing period of 4 – 16 ms before ^{13}C-^{13}C correlation spectra were measured.

Two types of long-distance experiments were conducted to probe the three-dimensional fold and self-assembly of the MPER-TMD in the lipid membrane. Intramolecular ^{13}C-^{19}F distances between 5F-W678 and L684 and I686 Cα were measured using a frequency-selective REDOR experiment [40]. An 800 μs Gaussian ^{13}C π pulse was applied in the middle of the REDOR period to invert the ^{13}C spin of interest and to suppress ^{13}C-^{13}C scalar couplings. The REDOR mixing time ranged from 5 ms to 25 ms, and the experiments were conducted under 5 kHz MAS at 235 K to immobilize the peptide.

Intermolecular distances were measured using the ^{19}F CODEX experiment [41-43]. Two trains of ^{19}F 180° pulses spaced every half a rotor period were applied before and after a longitudinal mixing period. The ^{19}F 180° pulses recouple the ^{19}F chemical shift anisotropy

(CSA) and cause the formation of a stimulated echo. ^{19}F spin diffusion during the mixing period due to oligomerization decreases the echo intensity. To correct for T_1 relaxation effects, two experiments, a control (S_0) and a dephasing (S) experiment, in which the mixing time was interchanged with a z-filter after the second π-pulse train, were measured, and the intensity ratio S/S_0 indicates the extent of ^{19}F spin diffusion. The ^{19}F CODEX experiments were conducted under 8 - 10 kHz MAS at 233 K, in order to immobilize the peptide and ensure detection of only spin diffusion and not slow motion [43].

To investigate the mobility of the MPER-TMD in the lipid membrane, we measured ^{13}C-^{1}H dipolar couplings using a 2D double-quantum-filtered (DQF) DIPSHIFT experiment [44-46]. FSLG [47] was used for ^{1}H homonuclear decoupling and SPC5 [48] was used for ^{13}C-^{13}C recoupling and double-quantum filtering. The experiment was conducted under 7 kHz MAS at 303 K. The time-domain data were fitted to obtain the apparent couplings, which were divided by the FSLG scaling factor of 0.577 to obtain the true couplings. The C-H order parameter S_{CH} was calculated as the ratio of the true coupling to a rigid-limit value of 22.7 kHz.

Static ^{31}P spectra of lipid membranes were measured at 298 K to investigate the effects of MPER-TMD on membrane morphology [49-51]. To determine the effect of the peptide on the membrane-surface hydration, we measured 2D ^{1}H-^{31}P heteronuclear correlation (HETCOR) spectra at 298 K under 5 kHz MAS using a 100 ms ^{1}H mixing time [52-55].

Simulation of ^{19}F CODEX and ^{13}C-^{19}F REDOR intensities

The ^{19}F CODEX S/S_0 intensities were fit using a home-written MATLAB program to obtain ^{19}F-^{19}F distances [43]. The program uses the exchange matrix formalism to treat multi-spin diffusion. For trimeric systems, the 3 × 3 exchange matrix contains rate constants that are proportional to an overlap integral and the ^{19}F dipolar coupling of interest. Based on model compound results, the value of the overlap integral is 37 μs at 8 kHz MAS and 41 μs at 10 kHz MAS [42]. To simulate F699 distances, we considered two oligomeric structures: 50% of an α-helical trimer and 50% of a β-sheet consisting of three parallel β-strands. The inter-strand distances were adjusted to 5.8 and 6.8 Å for the POPE and VMS data, respectively, in order to fit the fast initial decay, while the inter-helical distances were varied to fit the slow decay at longer mixing times. ^{13}C-^{19}F REDOR S/S_0 intensities were fit using the SIMPSON program [56] to obtain intramolecular distances. An intensity scaling factor of 0.85 was applied to the calculated curves to represent ^{19}F pulse imperfections in the REDOR data [57].

Structural modeling of the MPER-TMD trimer

We carried out molecular dynamics (MD) simulations in explicit membranes to assess the energetic stability of the MPER-TMD trimer structures in lipid bilayers and to obtain a view of the turn structure between the MPER and TMD. We used the monomer structure of the Ebola virus envelope glycoprotein (GP2) MPER-TMD (PDB code: 5T42) [21] as the initial template, and substituted the Ebola sequence with the gp41 sequence (residues K665 – I704) by aligning P653 in the Ebola protein with one of seven residues in gp41 (L684, K683, I682, Y681, W680, L679, and W678) (Tables S1, S2). The (ϕ ψ) angles of two solution NMR structures (PDB: 5JYN and 6B3U) were then applied to the TMD residues I688-I697 in the

model. Each monomer was trimerized, then inserted into a lipid bilayer containing 60 POPC, 30 POPE, 30 POPS, 20 SM, and 60 cholesterol molecules. This membrane matches the composition of the VMS membrane used in the experiments, and was created using the Charmm-Gui Membrane Builder [58]. The simulation box, obtained from the CHARMM-GUI website server, consists of 7750 TIP3 waters and 21 potassium ions. MD simulations were carried out in Gromacs [59] using measured ^{13}C-^{19}F and ^{19}F-^{19}F distance constraints. In addition to these experimental constraints, we fixed N – N, Cα – Cα, and C' – C' distances between residue *i* and residue *i*+4 for residues K683–S703 to maintain the TMD backbone conformation (Tables S3). During the simulations, we found that the three intermolecular ^{19}F-^{19}F restraints were insufficient to stabilize the trimer; therefore, we added three interhelical restraints of 9.4 Å, 6.5 Å, and 8.0 Å at G690 Cα, V693 Cα, and R696 Cα, obtained from the solution NMR structure of trimeric TMD (PDB: 5JYN), to help stabilize the trimer [19]. The energy of the system was minimized using a steepest decent strategy followed by a six-step equilibration process at 303 K for 3.75 ns. After equilibration, the production run was carried out at the same temperature for 100 ns.

Results

MPER-TMD is fusogenic and is predominantly α-helical in lipid membranes

To determine the three-dimensional fold and oligomeric structure of gp41 MPER-TMD in lipid membranes, we synthesized a 40-residue peptide corresponding to residues 665-704 of the HXB2 isolate of gp41 (Table 1). ^{13}C, ^{15}N-labeled residues and ^{19}F-labeled residues were placed at strategic positions in the peptide (Table 2) to investigate the conformation and intermolecular assembly of this domain. A semi-automated continuous-flow Fmoc peptide synthesis protocol was used to allow each amino acid to be incorporated into the sequence every 3~4 minutes. CD spectra of the peptide in POPC/POPG and DOPC/DOPE vesicles showed α-helical conformations, with slightly lower helical content in the DOPC/DOPE membrane (Fig. S1B). This trend is consistent with the conformation of the PIV5 fusion protein TMD, which showed a pronounced membrane-induced conformational change from α-helix in lamellar bilayers to β-sheet in negative-curvature phosphatidylethanolamine (PE) membranes [55]. To determine whether the MPER-TMD is fusogenic, we carried out fluorescence lipid mixing assays. MPER-TMD caused rapid mixing of POPC/POPG (4:1) vesicles (Fig. S1C): ~50% of the vesicles undergo mixing in less than 30 s, and by 10 minutes the extent of mixing increased to ~75%. Therefore, the MPER-TMD peptide is fusogenic in vitro.

2D ^{13}C-^{13}C correlation spectra provided information about the backbone conformation of the peptide in lipid membranes. We prepared a cholesterol-containing membrane (VMS) to mimic the virus envelope, and a POPE membrane to investigate the effect of membrane curvature on peptide conformation. Fig. 2 shows that L669 in the MPER and L684, I686, and G694 in the TMD exhibit exclusive α-helical chemical shifts in both membranes. In comparison, the C-terminal residue A700 shows a weak β-strand Cα-Cβ cross peak in addition to the α-helical cross peak in the VMS membrane (Fig. 2A). The POPE membrane increased the β-strand cross peak intensity to be comparable to the intensity of the α-helical peak (Fig. 2B). Thus, the C-terminus of the TMD has a moderate propensity to form β-

strand structures in lipid membranes. These 2D spectra were measured at moderate low temperatures of 263 K to freeze the peptide motion and to obtain higher sensitivity. Comparison of the 1D ^{13}C spectra at 303 K and 235 K (Fig. 2D) indicate that the peptide has the same chemical shifts between physiological temperature and low temperature, thus the structure is unchanged within this temperature range, and the structural constraints measured at the low temperatures used here also apply to the physiological temperature.

Depths of insertion of the MPER-TMD in lipid bilayers

We next investigated the depth of insertion of MPER-TMD by correlating the lipid and water ^{1}H chemical shifts with the protein ^{13}C chemical shifts in a 2D experiment [34]. Fig. 3A shows a representative 2D spectrum, measured using a ^{1}H spin diffusion mixing time of 400 ms, for the LWIGA-labeled peptide bound to the POPE membrane. At this long mixing time, all ^{13}C-labeled residues show cross peaks with both water and lipid CH_2 protons. The different depths of insertion of the residues can be discerned from the relative intensities of their water versus lipid CH_2 cross peaks.

Fig. 3B shows the ^{1}H cross sections of L669 Cα and Cβ at various ^{1}H mixing times. It can be seen that the water cross peak intensity has equilibrated by 100 ms while the lipid-chain cross peak is weak and continues to grow till the longest mixing time of 400 ms. In comparison, the I686 cross sections show significantly higher lipid cross peaks compared to L669. Fig. 3C shows the ^{13}C cross sections at the lipid CH_2 and water ^{1}H chemical shifts from the 9 ms 2D spectrum, illustrating the different relative intensities of lipid and water cross peaks for different residues. Fig. 3D summarizes this information as polarization transfer curves from water to protein and from lipid chains to protein. The lipid-to-protein buildup curves show significant differences between residues: I686 has the fastest polarization transfer from the lipids while L669 has the slowest transfer. The difference between the water polarization transfer is less pronounced, but still shows the expected opposite trend. Together, these data indicate that I686 is the most membrane-embedded residue, followed by A700 near the C-terminus of the TMD, whereas L669 lies on the membrane surface, the furthest away from the middle of the bilayer.

Since the water-to-protein polarization transfer curves do not differ significantly between residues from the ^{1}H-^{13}C correlation experiment, we measured water-edited 2D ^{13}C-^{13}C correlation spectra to better distinguish the water accessibilities of different residues [37-38]. Fig. S2 show 2D ^{13}C-^{13}C correlation spectra of LWIGA-labeled peptide in POPE and VMS membranes. The water-edited spectra were measured using a short ^{1}H T_2 filter of 0.6 – 0.8 ms, followed by a ^{1}H spin diffusion mixing time of 4 – 16 ms. At these short ^{1}H mixing times, most of the ^{1}H polarization comes from water. For both POPE and VMS membrane samples, L669 shows the highest residual intensities in the water-edited 2D spectra, followed by A700, whereas I686 cross peaks are mostly removed. Therefore, the water-edited spectra are fully consistent with the 2D ^{1}H-^{13}C correlation spectra in showing that L669 is the most exposed to aqueous solution whereas I686 is the most buried in the lipid bilayer. The intensity ratios of the water-edited spectra and the control spectra (Fig. S2C) are lower for the POPE-bound peptide than for the VMS-bound peptide at the same mixing time of 9 ms,

suggesting that the peptide may dehydrate the POPE membrane more than the VMS membrane.

MPER-TMD causes negative Gaussian curvature to PE membranes

To obtain information about the interaction of the MPER-TMD with lipid membranes, we measured ^{31}P static and MAS spectra. Static ^{31}P lineshapes of four membranes in the absence and presence of the peptide are shown in Fig. S3A. POPC/POPG and VMS membranes exhibit uniaxial powder lineshapes that are similar with or without the peptide, indicating that MPER-TMD does not perturb the lamellar structure of these membranes. For comparison, the peptide caused a small isotropic peak to the POPE membrane. The peptide-free DOPE membrane shows a powder lineshape that is characteristic of an inverted hexagonal phase (H_{II}), as expected for this lipid, while the peptide-bound DOPE membrane exhibits a dominant isotropic peak. We have shown before that this isotropic peak is indicative of negative Gaussian curvature [55, 60], which is essential for membrane remodeling during hemifusion and post-fusion stages of the virus-cell fusion. This negative Gaussian curvature has also been observed in other membrane-active peptides [49-50] and has been quantified using small-angle X-ray scattering experiments [61-62].

Since membrane dehydration is expected at some stages of viral fusion, we investigated the membrane-surface hydration of the POPE and VMS membranes using 2D ^{1}H-^{31}P correlation experiments. Fig. S3B shows that the lipid phosphate groups of both membranes have a strong water cross peak, indicating that both membranes remain well hydrated in the presence of the MPER-TMD. This behavior differs from the PIV5 fusion protein TMD, which significantly dehydrates PE membranes in which the peptide is predominantly β-strand. We attribute the high hydration to the α-helical conformation of the MPER-TMD, and suggest that the β-strand conformation is correlated with membrane dehydration.

MPER-TMD is immobilized in lipid membranes

Information about the three-dimensional fold and oligomeric state of the MPER-TMD in the membrane can be obtained from peptide dynamics, since a monomeric membrane-spanning α-helix is expected to undergo rapid uniaxial diffusion in the membrane [63-65] while a highly oligomerized peptide or a peptide that contains an extended segment on the membrane surface is expected to be immobilized [66-67]. We measured the ^{13}C-^{1}H dipolar order parameters of LWIGA-labeled MPER-TMD in the VMS membrane at 303 K using a double-quantum-filtered (DQF) 2D DIPSHIFT experiment [46]. The double-quantum filter removes the lipid natural abundance ^{13}C signals, which partly overlap with the peptide ^{13}C peaks (Fig. 4A). The resulting Cα-Hα dipolar dephasing curves (Fig. 4B) indicate relatively large C-H order parameters of 0.89 – 0.92 for both the MPER residue L669 and the TMD residues I686 and A700, indicating that both the MPER and TMD are immobilized in the membrane. This suggests that the MPER-TMD may be oligomerized in the membrane. To directly determine the oligomeric state of the protein, we next carried out the spin-counting ^{19}F CODEX experiment [41].

MPER-TMD is trimerized in the lipid bilayer and has a turn between the MPER and TMD

We measured the oligomeric state of MPER-TMD in lipid bilayers by taking advantage of the presence of many aromatic residues, which can be readily fluorinated. The ^{19}F CODEX experiment reports the number of ^{19}F spins in close proximity in terms of the T_1-corrected intensity (S/S_0) of a stimulated echo at equilibrium [41]. A trimeric complex with ^{19}F-^{19}F distances within about 15 Å should manifest equilibrium echo intensities of 1/3, while a monomer should have a full echo intensity of 1. To prevent slow motion from contributing to the exchange effect during the mixing time, we conducted the CODEX experiments at 233 K [43, 67]. ^{13}C chemical shifts measured at 235 K and 303 K show no differences (Fig. 2D), indicating that the MPER-TMD structure is unchanged in this temperature change. We introduced 4F-F699 in the TMD and 5F-W678 and 5F-W680 in the MPER to measure the oligomeric state and potential intermolecular distances (Fig. 5A). When the 4F-F699 labeled peptide was reconstituted into the membranes at a P/L ratio of 1 : 15, the CODEX intensities decayed to 0.32±0.07 for the POPE-bound peptide and 0.35±0.07 for the VMS membrane-bound peptide (Fig. 5B, C). Therefore, these data directly prove that the MPER-TMD is trimerized in both POPE and VMS membranes. In comparison, the W678 and W680 CODEX data show higher equilibrium values. For example, at a mixing time of 2 s, the W680 S/S_0 ratio is 0.51 ± 0.07 in the POPE membrane and 0.64±0.08 in the VMS membrane. But since the F699 result dictates that the MPER-TMD forms trimers, the Trp CODEX data must be fit to a three-spin model, albeit with longer internuclear distances. Both W680 and W678 CODEX decays are single exponential. Using a symmetric trimer model, we obtained best-fit distances of 11.0 Å for POPE-bound W680 and 12.0 Å for the VMS-bound peptide (Fig. 5D). The VMS membrane-bound W678 exhibits similar decay rate as that of W680, with a best-fit distance of 12.0 Å (Fig. 5E).

Compared to the two Trp residues' CODEX decays, the 4F-F699 CODEX data in both POPE and VMS membranes show an initial fast decay and a slow decay at longer mixing times, with approximately equal weights. We attribute this bi-exponential decay to the conformational heterogeneity at A700, which exhibits β-strand and α-helical chemical shifts with similar intensities. Therefore, we fit the F699 CODEX data using a two-component model, in which a linear chain of three spins, representing parallel in-register β-strands, is combined with a symmetric trimer, representing a three-helix bundle. The inter-strand distance was adjusted to fit the initial decay while the interhelical distance was adjusted to fit the slow decay. We obtained a best-fit interhelical distance of 11.0 Å for the POPE-bound peptide and 11.5 Å for the VMS-bound peptide. The inter-strand distance that accounts for the initial fast decay is 5.8 Å for the POPE-bound peptide and 6.8 Å for the VMS-bound peptide (Fig. S4). These inter-strand distances are longer than the backbone separation of ~4.7 Å in cross-β amyloid fibrils, which may result from sidechain disorder for the Phe rings or loose association of the β-strand at the C-terminus of the peptide due to spatial constraints by the rest of the peptide. We note that this two-conformation model does not affect the trimer conclusion, since any deviation from the trimer model in either the helix or the strand population of the peptide would change the CODEX equilibrium value from the measured value of ~0.33.

To investigate whether the oligomeric state of MPER-TMD is sensitive to the peptide concentration in the membrane, we prepared another POPE-bound sample with a three-fold lower P/L ratio of 1 : 45, and measured the CODEX data. Fig. 5C shows that this diluted peptide sample has similar CODEX intensities to the 1 : 15 sample, thus indicating that the MPER-TMD trimer is insensitive to the peptide concentration within the concentration range studied here.

To investigate whether a turn is present between the MPER and TMD, we measured ^{13}C-^{19}F distances between 5F-W678 and ^{13}C-labeled I686 and L684 in the WLIGF-labeled peptide, and between 5F-W680 and ^{13}C-labeled I686 in LWIGA-labeled peptide. If a turn exists between the MPER and TMD, then the intramolecular distances are expected to be shorter than those of a continuous helix. Various structures of truncated constructs of gp41 containing part of the MPER or part of the TMD indicate distances longer than 13 Å between the W678 sidechain and the L684 and I686 backbone, which are too long to be detectable by ^{13}C-^{19}F dipolar couplings. In the W680-fluorinated LWIGA sample, I686 Cα exhibits negligible dephasing by 5F-W680 (data not shown), indicating that the distance is longer than 13 Å. In contrast, I686 and L684 Cα are clearly dephased by 5F-W678. Fig. 6 shows the frequency-selective ^{13}C-^{19}F REDOR data of WLIGF-labeled MPER-TMD bound to the VMS membrane. Representative S_0 and S spectra of the Cα region (Fig. 6A) show significant intensity differences without and with ^{19}F pulses, indicating detectable dipolar couplings. The normalized REDOR intensities (S/S_0) for the two Cα carbons (Fig. 6B) decay to ~0.50 for I686 Cα and ~0.75 for L684 Cα by 25.6 ms. To fit the experimental dephasing curves, we took into account the ^{19}F CSA of 47.5 ppm for 5F-W678 and ^{19}F 180° pulse imperfections [57, 68-69]. Best-fit simulations gave a distance of 9.2 Å for 5F-W678 to I686Cα and 10.0 Å for 5F-W678 to L684Cα.

Based on these ^{13}C-^{19}F and ^{19}F-^{19}F distances and the depths of insertion of different residues, we built a trimer model of MPER-TMD to assess the energetic stability of the trimer in lipid membranes and to obtain a low-resolution view of its structure. Since the ^{1}H-^{13}C correlation spectra place the MPER L669 on the membrane surface and the TMD I686 in the membrane interior, we used the helix-turn-helix structure of the Ebola GP2 MPER-TMD (PDB code: 5T42) as the initial structure template [21]. To define the turn position between the MPER and TMD, we aligned the gp41 sequence with the Ebola sequence in seven ways, matching each residue between L684 and W678 in MPER with the Ebola residue P653 (Table S1). Using the two dominant rotamers of t90 ($\chi_1 = \pm 180°$, $\chi_2 = +90°$) and t-105 ($\chi_1 = \pm 180°$, $\chi_2 = -105°$) for the W678 sidechain [70], we found that template E, matching W680 with P653, gave good agreement with the measured ^{13}C-^{19}F distances between 5F-W678 and L684 and I686 Cα, while other alignments produced distances or secondary structures that deviated significantly from experimental data (Table S2). For example, matching L684 of gp41 with P653 (template A) resulted in long distances of 14-16 Å from L684Cα and I686Cα to 5F-W678. Matching P653 with K683 (template B), which is traditionally considered the boundary between the MPER and TMD, caused either long distances or non-helical structures of I684 and L686. In this way, we ruled out four of the seven templates. The three remaining alignments were subjected to MD simulations under the constraints of the measured ^{13}C-^{19}F and ^{19}F-^{19}F distances. Based on the W680-P653 alignment (template E), we generated two monomer models by using the backbone (ϕ

ψ) torsion angles from the recently reported solution NMR structures of gp41 TMD (5JYN [19] and 6B3U [23]) for residues I688–I697. The resulting helix-turn-helix monomers were each trimerized, inserted into a lipid bilayer with the composition of the VMS membrane, and subjected to 100 ns MD simulations [59] in Gromacs under the constraints of the measured ^{13}C-^{19}F and ^{19}F-^{19}F distances. Specifically, the intramolecular 5F-W678 to L684Cα distance and 5F-W678 to I686Cα distance are 10.0 Å and 9.2 Å, respectively, while the intermolecular ^{19}F-^{19}F distances at residues W678, W680, and F699 are 12.0 Å, 12.0 Å, and 11.5 Å in the VMS membrane, respectively (Table 3). In addition, we fixed backbone Cα – Cα, N - N, and C' – C' distances between residues *i* and *i* + 4 of the TMD (from K683 to S703) to stabilize the monomer conformation during simulations (Table S3). We also introduced three additional intermolecular distance restraints at G690 Cα, V693 Cα, and R696 Cα, obtained from the PDB structure 5JYN, to help stabilize the trimer assembly.

The results of these simulations based on the template-E alignment are shown in Fig. 7 and Fig. S6. Both structural models point W678 towards the helix-helix interface and W680 towards solution. The two Trp residues predominantly adopt t90 and t-105 rotamers (Table S4) [70]. Residues W678 to K683 show non-helical torsion angles (Fig. S5), but most MPER residues retain the α-helical (ϕ ψ) angles from the input values, without changing to non-helical structures during the 100 ns simulations. The L669 sidechain faces the membrane, consistent with the observed lipid cross peaks of this residue. Moreover, the 5F-W680 to I686Cα distance is longer than 16 Å in both models, in good agreement with the negligible dipolar dephasing between 5F-W680 and I686 in the REDOR experiments.

While these simulations based on the W680-P653 alignment gave structures that agree with the experimental data, simulations using the Y681-P653 alignment (template D) and the W678-P653 alignment (template G) did not (Fig. 8). The template-D structure shows a short distance of less than 7 Å between 5F-W680 and I686Cα, which contradicts the experimental data. The template-G alignment produced a trimer structure in which L669 points to aqueous solution while W680 is embedded in the lipid bilayer, with a distance of less than 7 Å to I686 Cα. Both features disagree with the experimental data. Therefore, residues Y681 and W678 do not correspond to the turn positions and these alternative structural models can be ruled out.

Discussion

Oligomeric state and three-dimensional fold of gp41 MPER-TMD in lipid membranes

The ^{19}F CODEX data of 4F-F699, showing equilibrium intensities of ~0.33 (Fig. 5B, C), unambiguously indicate that the MPER-TMD self-associates into trimers in lipid membranes at peptide concentration of 2–7 mol%. This trimerization is observed in both lamellar virus-mimetic membranes containing 30% cholesterol and in negative-curvature POPE membranes. Trimer formation in the absence of the water-soluble ectodomain suggests that this C-terminal region of gp41 may be the trimerization core of the protein, and may stabilize the trimeric state of the ectodomain [71-72]. Trimerization is also consistent with the high Cα-Hα dipolar order parameters of two TMD residues and one MPER residue (Fig. 4). These high and similar order parameters indicate that only small-amplitude local motions are present, while fast uniaxial rotational diffusion of the entire peptide is absent. The latter

is true because the TMD and MPER residues have very different Cα-Hα bond orientations relative to the bilayer normal, thus they would give rise to very different order parameters if whole-body uniaxial diffusion were present [64, 73].

Intramolecular ^{13}C-^{19}F distance measurements provided important constraints about the relative orientation of the TMD and MPER. If the two segments form a continuous α-helix, as reported in a number of structural studies (Fig. 1), then distances of 11-19 Å would be expected between the W678 sidechain and L684 and I686 backbone (Fig. 6D). Instead, we measured ^{13}C-^{19}F distances of 10.0 Å and 9.2 Å, which constrain W678 to be part of a turn that deposits the MPER onto the membrane surface. The helix-turn-helix fold is supported by the fact that L669 is not only well exposed to water but also shows cross peaks with lipid acyl chains at ^{1}H spin diffusion mixing times of 100 ms (Fig. 3). If the MPER segment were to extend away from the membrane surface into the aqueous solution, then L669 would not be in spin diffusion contact with the lipid chains [34, 74-75]. Finally, the helix-loop-helix architecture is also consistent with the observed immobilization of the MPER-TMD. Taken together, the distance data and the depth of insertion data define the three-dimensional fold and oligomeric state of the gp41 MPER-TMD as a trimeric helix-turn-helix structure (Fig. 7). The umbrella-like structural topology is held together by the trimeric membrane-spanning TMD stalk, while the MPER fans out on the membrane surface.

The surface location of MPER is fully consistent with the Trp-rich (W666, W670, W672, W678, and W680) nature of MPER, since Trp residues are known to favor the membrane-water interface due to the nonpolar aromatic ring and the ability of the indole NH to hydrogen-bond with lipid carbonyls and phosphate oxygens [76-77]. Indeed, the solution NMR structure of DPC-bound MPER peptide shows that most Trp residues face the membrane interior while the polar residues in this segment face the aqueous solution (Fig. 1C). Thus, the helix-turn-helix structure of the MPER-TMD is favorable for stabilizing both the Trp-rich amphipathic MPER helix and the hydrophobic TMD helix. The topology of the gp41 MPER-TMD resembles the pinwheel structure of the pentameric phospholamban (PLN), which regulates calcium homeostasis in cardiac muscles. There, orientational NMR measurements, paramagnetic relaxation enhancement data, and DEER distance data, indicate that the N-terminal cytoplasmic domain of PLN lies on the membrane surface while a C-terminal TMD spans the bilayer [78-79].

While the present data clearly define the tertiary and quaternary structures of the MPER-TMD, they do not uniquely constrain the turn structure between W678 and K683 at the atomic level. For example, slightly different TMD backbone conformations cause different rotamers of W678 and W680, which all agree with the measured ^{13}C-^{19}F distances and ^{19}F-^{19}F distances (Fig. 7 and Fig. S6). Further experiments measuring the ^{13}C and ^{15}N chemical shifts and many interresidue contacts will be necessary to fully determine the atomic-resolution structure of this turn between the MPER and TMD.

Comparison of the oligomeric structure in lipid bilayers with previous structures in bicelles

The trimeric helix-turn-helix structural model obtained from the current study differs from two solution NMR structures of gp41 (residues 677-716), but in different ways [19, 23]. The

previous construct, denoted TMD-CT below, includes six MPER residues, the TMD, and ten residues of the cytoplasmic domain. Both structures were solved in small bicelles with DMPC to DHPC molar ratios of 1 : 2 to 1 : 2.5 (q = 0.4-0.5). One study, conducted at a P/L molar ratio of 1 : 225, concluded a trimeric structure based on intermolecular ^{15}N-^{1}H NOE's between ^{13}C, ^{1}H-labeled protein and ^{15}N, ^{2}H-labeled protein [19]; however assignment of the methyl ^{1}H chemical shifts is ambiguous. In contrast, the second study, conducted at a P/L molar ratio of 1 : 300, found that residual dipolar couplings of the protein in different alignment media disagree with C_3 symmetry; paramagnetic relaxation enhancement data show no intermolecular association, and DEER EPR data at P/L ratios of 1 : 4000 to 1 : 300 also indicate an absence of intermolecular dipolar couplings [23]. Therefore these data indicate a monomeric helix in these small bicelles [23]. We speculate that these divergent findings may result from heterogeneity in the protein oligomeric states, differences in the bicelle stability and size, and the different P/L ratios used. At the higher P/L ratio of 1 : 225, an oligomeric population may coexist with a monomeric population to give rise to the intermolecular NOE's, while the lower P/L ratios may shift the protein conformational equilibrium to the monomeric state.

The experimental conditions in the current study promote more stable membrane environments as well as more stable protein structures compared to the conditions of these solution NMR studies. First, the current gp41 construct includes the entire MPER region in addition to the entire TMD. The Trp-rich MPER is expected to have significant propensity for binding to the membrane surface [20], which should tether the protein to the membrane to increase the probability for oligomerization. Second, the phospholipids in the current study present essentially an infinite membrane plane with weak curvature, thus placing no spatial restrictions on potential trimer formation. In comparison, the q = 0.4-0.5 DMPC/DHPC bicelles in the solution NMR studies have an average width of only ~45 Å for the flat portion of the bicelle, which is capped by the round DHPC edges [19]. The thickness of the bilayer portion is only ~30 Å, dictated by the DMPC chain length. This restricted volume may shift the protein structural equilibrium towards the monomeric state. Third, the current solid-state NMR experiments use relatively high P/L molar ratios of 1 : 15 to 1 : 45 to obtain sufficient sensitivity, which should shift the equilibrium towards trimers. Future experiments are required to address the question of whether the MPER-TMD remains trimeric at much lower P/L ratios in lipid bilayers. It is informative to review existing biochemical and biophysical evidence for the environmental dependence of the oligomerization of viral fusion protein TMDs. Analytical ultracentrifugation data of the PIV5 fusion protein TMD [80] indicate weak homo-oligomerization tendency in DPC micelles. In comparison, oxidative crosslinking of Cys mutants of full-length PIV5 F protein in HeLa cell membranes show cross-linking even at very low protein concentrations [81]. Solution NMR studies of full-length gp41 at low protein : detergent molar ratios of 1 : 500 detected only signals of the N-terminal ~110 residues, indicating that the C-terminal MPER and TMD are immobilized, which suggest oligomerization [15]. Analytical ultracentrifugation and liposome release assay of a series of gp41 constructs in DPC micelles found that the oligomeric state depended on pH, construct length, and P/L ratios in a complex manner [18]. Trimer formation is favored by high pH and by inclusion of the water-soluble ectodomain heptad repeats. At a very low protein : DPC molar ratio of ~1 : 3000, a construct that includes both the ectodomain heptad

repeats and the MPER-TMD was found to be trimeric at high pH while monomeric at low pH.

Backbone conformation of the MPER-TMD protomer

Since most structural studies of MPER and TMD peptides found α-helical conformations, we sparsely labeled our peptide with ^{13}C, ^{15}N-labeled residues, with the goal of assessing the influence of the membrane on the peptide backbone conformation. Out of the labeled residues, only A700 at the C-terminus of the TMD exhibits partial β-strand conformation. The β-strand peaks account for ~50% of the total intensities of this residue in POPE membranes, while in the VMS membrane the β-strand peak intensities were initially low and gradually equilibrated to ~50%. Similarly, PE membranes induced β-strand conformation of the PIV5 fusion protein TMD [55], but the β-strand chemical shifts are observed for more residues in the peptide. We attribute the partial β-strand character of the gp41 TMD to a combination of the amino acid sequence and the spontaneous negative curvature of PE membranes. It has been shown that membrane peptides rich in β-branched Ile and Val residues have a significant propensity for the β-sheet conformation [82-84]. Both PIV5 and HIV fusion protein TMDs contain ~40% Ile and Val residues, thus isolated TMD peptides in lipid membranes with the appropriate curvature may have a significant tendency to change to the β-strand conformation. The presence of the MPER in the current study may have shifted the conformational equilibrium towards the α-helix, thus restricting the β-strand segment to the C-terminal end of the TMD. In analogy, a FP-TMD chimera of the PIV5 fusion protein also exhibited membrane-independent α-helical conformation for the entire protein [85]. Additional studies are necessary to understand the significance of the C-terminal β-strand conformation for virus-cell fusion. It is noteworthy that the N-terminal fusion peptide of gp41 has been shown to adopt β-strand conformation in complex cholesterol-containing membranes [86-87]. Thus, we speculate that the β-sheet structures of both domains may promote close association of the FP and TMD in the lipid membrane, to cause the necessary saddle-splay curvature [55, 61] in late stages of membrane fusion.

Implication of the trimeric helix-turn-helix structural motif for HIV membrane fusion

The trimeric helix-turn-helix structure of the gp41 MPER-TMD in lipid bilayers has two implications for the mechanism of HIV virus-cell membrane fusion. First, the segment from W678 to K683 may be a site of conformational plasticity, and the turn conformation may be important for the protein to interact with lipid components such as PE and cholesterol to induce membrane curvature. The ^{31}P lineshapes (Fig. S3) confirm membrane-curvature induction by the MPER-TMD. In support of this notion, recent lipid mixing assays showed that only a peptide that spans the junction between the MPER and TMD (residues 671-693) has fusogenic activity, while peptides corresponding only to the MPER (residues 656-683) or only to the TMD (residues 684-705) are not fusogenic [88]. The fusion activity of the MPER-TMD junction not only increases with the peptide concentration but also increases with the cholesterol concentration. MD simulations suggest that this cholesterol dependence may arise from the stabilizing effect of cholesterol to focal points of negative curvature created by the aromatic-rich residues between the MPER and TMD, which cause phospholipid protrusion and acyl-chain splay to promote membrane fusion [88]. Among anti-MPER antibodies, the two most broadly reactive antibodies, 4E10 and 10E8, both bind to

residues spanning the MPER-TMD junction. For example, the epitope residues recognized by 10E8 include W672, F673, W676 as well as K/R683 in the turn [7]. The precise interactions among 10E8, the turn between the MPER and TMD, and the lipids, are currently unknown. Crystal structures of 10E8 in complex with an MPER peptide and short-chain lipids have recently been reported [89], suggesting that the 10E8 epitope may consist of both the MPER and lipids.

Second, the surface orientation of the MPER helix, detected from the 2D ^{1}H-^{13}C correlation spectra and water-edited 2D ^{13}C-^{13}C correlation spectra, may be important for recognition of the N-terminal fusion peptide proximal region (FPPR) during late stages of virus-cell fusion. Fluorescence resonance energy transfer and lipid mixing data indicate that the TMD and FP of gp41 interact with each other in lipid membranes [90]. This implies that their respective neighboring segments of the MPER and FPPR may also interact with each other after the formation of the ectodomain six-helix bundle. For the Ebola virus fusion protein, titration of the FP caused chemical shift perturbation of the surface-bound MPER residues [21], also supporting an interaction between the MPER and N-terminal regions of the fusion protein. Future studies determining the atomic-resolution structure of the MPER-TMD in lipid membranes will be required to understand the precise mechanistic roles of this domain for HIV entry into cells.

Supplementary Material

Refer to Web version on PubMed Central for supplementary material.

Acknowledgments

The authors thank Professor Barbara Imperiali, Dr. Jean-Marie Swiecicki and Dr. Debasis Das for help with lipid mixing assays, and Mr. Alex Shcherbakov for helpful discussions about REDOR simulations and structural modeling. This work is supported by NIH grant GM066976 to M.H. The structural model in Figure 7 is deposited at the Protein Data Bank (accession code: 6DLN; BMRB code 30472). The alternative structural model in Figure S6 is available upon request to meihong@mit.edu.

References

1. Eckert DM; Malashkevich VN; Hong LH; Carr PA; Kim PS, Inhibiting HIV-1 entry: Discovery of D-peptide inhibitors that target the gp41 coiled-coil pocket. Cell 1999, 99 (1), 103–115. [PubMed: 10520998]
2. Chan DC; Kim PS, HIV entry and its inhibition. Cell 1998, 93, 681–684. [PubMed: 9630213]
3. Weissenhorn W; Dessen A; Harrison SC; Skehel JJ; Wiley DC, Atomic structure of the ectodomain from HIV-1 gp41. Nature 1997, 387, (387) 426–430. [PubMed: 9163431]
4. Chan DC; Fass D; Berger JM; Kim PS, Core structure of gp41 from the HIV envelope glycoprotein. Cell 1997, 89, (2), 263–273. [PubMed: 9108481]
5. Harrison SC, Viral membrane fusion. Nature Struc. Mol. Biol 2008, 15, 690–698.
6. Lamb RA; Jardetzky TS, Structural basis of viral invasion: lessons from paramyxovirus F. Curr. Opin. Struct. Biol 2007, 17, 427–436. [PubMed: 17870467]
7. Huang JH; Ofek G; Laub L; Louder MK; Doria-Rose NA; Longo NS; Imamichi H; Bailer RT; Chakrabarti B; Sharma SK; Alam SM; Wang T; Yang YP; Zhang BS; Migueles SA; Wyatt R; Haynes BF; Kwong PD; Mascola JR; Connors M, Broad and potent neutralization of HIV-1 by a gp41-specific human antibody. Nature 2012, 491, (7424), 406–412. [PubMed: 23151583]

8. Buzon V; Natrajan G; Schibli D; Campelo F; Kozlov MM; Weissenhorn W, Crystal Structure of HIV-1 gp41 Including Both Fusion Peptide and Membrane Proximal External Regions. PLoS Pathog 2010, 6 (5).

9. Irimia A; Sarkar A; Stanfield RL; Wilson IA, Crystallographic Identification of Lipid as an Integral Component of the Epitope of HIV Broadly Neutralizing Antibody 4E10. Immunity 2016, 44, (1), 21–31. [PubMed: 26777395]

10. Montero M; van Houten NE; Wang X; Scott JK, The membrane-proximal external region of the human immunodeficiency virus type 1 envelope: dominant site of antibody neutralization and target for vaccine design. Microbiol. Mol. Biol. Rev 2008, 72, (1) 54–84, table of contents. [PubMed: 18322034]

11. Salzwedel K; West JT; Hunter E, A conserved tryptophan-rich motif in the membrane-proximal region of the human immunodeficiency virus type 1 gp41 ectodomain is important for Env-mediated fusion and virus infectivity. J. Virol 1999, 73, (3), 2469–2480. [PubMed: 9971832]

12. Miyauchi K; Komano J; Yokomaku Y; Sugiura W; Yamamoto N; Matsuda Z, Role of the specific amino acid sequence of the membrane-spanning domain of human immunodeficiency virus type 1 in membrane fusion. J. Virol 2005, 79, (8), 4720–4729. [PubMed: 15795258]

13. West JT; Johnston PB; Dubay SR; Hunter E, Mutations within the putative membrane-spanning domain of the simian immunodeficiency virus transmembrane glycoprotein define the minimal requirements for fusion, incorporation, and infectivity. J. Virol 2001, 75, (20), 9601–9612. [PubMed: 11559792]

14. Lin XX; Derdeyn CA; Blumenthal R; West J; Hunter E, Progressive truncations C terminal to the membrane-spanning domain of simian immunodeficiency virus Env reduce fusogenicity and increase concentration dependence of Env for fusion. J. Virol 2003, 77, (12), 7067–7077. [PubMed: 12768026]

15. Lakomek NA; Kaufman JD; Stahl SJ; Louis JM; Grishaev A; Wingfield PT; Bax A, Internal Dynamics of the Homotrimeric HIV-1 Viral Coat Protein gp41 on Multiple Time Scales. Angew. Chem. Int. Ed. Engl 2013, 52, (14), 3911–3915. [PubMed: 23450638]

16. Roche J; Louis JM; Aniana A; Ghirlando R; Bax A, Complete dissociation of the HIV-1 gp41 ectodomain and membrane proximal regions upon phospholipid binding. J. Biomol. NMR 2015, 61 (3-4), 235–248. [PubMed: 25631354]

17. Louis JM; Baber JL; Ghirlando R; Aniana A; Bax A; Roche J, Insights into the Conformation of the Membrane Proximal Regions Critical to the Trimerization of the HIV-1 gp41 Ectodomain Bound to Dodecyl Phosphocholine Micelles. PLoS One 2016, 11, (8), e0160597. [PubMed: 27513582]

18. Dai Z; Tao YS; Liu NN; Brenowitz MD; Girvin ME; Lai JR, Conditional Trimerization and Lytic Activity of HIV-1 gp41 Variants Containing the Membrane-Associated Segments. Biochemistry-Us 2015, 54 (8), 1589–1599.

19. Dev J; Park D; Fu QS; Chen J; Ha HJ; Ghantous F; Herrmann T; Chang WT; Liu ZJ; Frey G; Seaman MS; Chen B; Chou JJ, Structural basis for membrane anchoring of HIV-1 envelope spike. Science 2016, 353, (6295), 172–175. [PubMed: 27338706]

20. Sun ZY; Oh KJ; Kim M; Yu J; Brusic V; Song L; Qiao Z; Wang JH; Wagner G; Reinherz EL, HIV-1 broadly neutralizing antibody extracts its epitope from a kinked gp41 ectodomain region on the viral membrane. Immunity 2008, 28 (1), 52–63. [PubMed: 18191596]

21. Lee J; Nyenhuis DA; Nelson EA; Cafiso DS; White JM; Tamm LK, Structure of the Ebola virus envelope protein MPER/TM domain and its interaction with the fusion loop explains their fusion activity. Proc. Natl. Acad. Sci. U. S. A 2017, 114 (38), E7987–E7996. [PubMed: 28874543]

22. Apellaniz B; Rujas E; Serrano S; Morante K; Tsumoto K; Caaveiro JM; Jimenez MA; Nieva JL, The Atomic Structure of the HIV-1 gp41 Transmembrane Domain and Its Connection to the Immunogenic Membrane-proximal External Region. The Journal of biological chemistry 2015, 290 (21), 12999–13015. [PubMed: 25787074]

23. Chiliveri SC; Louis JM; Ghirlando R; Baber JL; Bax A, Tilted, Uninterrupted, Monomeric HIV-1 gp41 Transmembrane Helix from Residual Dipolar Couplings. J. Am. Chem. Soc 2018, 140, 34–37. [PubMed: 29277995]

24. Reardon PN; Sage H; Dennison SM; Martin JW; Donald BR; Alam SM; Haynes BF; Spicer LD, Structure of an HIV-1-neutralizing antibody target, the lipid-bound gp41 envelope membrane proximal region trimer. Proc. Natl. Acad. Sci. U. S. A 2014, 111 (4), 1391–1396. [PubMed: 24474763]
25. Chipot C; Dehez F; Schnell JR; Zitzmann N; Pebay-Peyroula E; Catoire LJ; Miroux B; Kunji ERS; Veglia G; Cross TA; Schanda P, Perturbations of Native Membrane Protein Structure in Alkyl Phosphocholine Detergents: A Critical Assessment of NMR and Biophysical Studies. Chem. Rev 2018, 118, 3559–3607. [PubMed: 29488756]
26. Back NK; Smit L; Schutten M; Nara PL; Tersmette M; Goudsmit J, Mutations in human immunodeficiency virus type 1 gp41 affect sensitivity to neutralization by gp120 antibodies. J. Virol 1993, 67, 6897–6902. [PubMed: 8411395]
27. Simon MD; Heider PL; Adamo A; Vinogradov AA; Mong SK; Li XY; Berger T; Policarpo RL; Zhang C; Zou YK; Liao XL; Spokoyny AM; Jensen KF; Pentelute BL, Rapid Flow- Based Peptide Synthesis. Chembiochem 2014, 15 (5), 713–720. [PubMed: 24616230]
28. Luo W; Cady SD; Hong M, Immobilization of the Influenza A M2 Transmembrane Peptide in Virus-Envelope Mimetic Lipid Membranes: A Solid-State NMR Investigation. Biochemistry-Us 2009, 48, 6361–6368.
29. Cady SD; Wang T; Hong M, Membrane-dependent effects of a cytoplasmic helix on the structure and drug binding of the influenza virus M2 protein. J. Am. Chem. Soc 2011, 133, 11572–11579. [PubMed: 21661724]
30. Lorizate M; Sachsenheimer T; Glass B; Habermann A; Gerl MJ; Kräusslich HG; Brügger B, Comparative lipidomics analysis of HIV-1 particles and their producer cell membrane in different cell lines. Cell. Microbiol 2013, 15, 292–304. [PubMed: 23279151]
31. Lee M; Yao H; Kwon B; Waring AJ; Ruchala P; Singh C; Hong M, Conformation and Trimer Association of the Transmembrane Domain of the Parainfluenza Virus Fusion Protein in Lipid Bilayers from Solid-State NMR: Insights into the Sequence Determinants of Trimer Structure and Fusion Activity. J. Mol. Biol 2018, 430, 695–709. [PubMed: 29330069]
32. Takegoshi K; Nakamura S; Terao T, ^{13}C-^{1}H dipolar-assisted rotational resonance in magic-angle spinning NMR. Chem. Phys. Lett 2001, 344 (5-6), 631–637.
33. Morcombe CR; Gaponenko V; Byrd RA; Zilm KW, Diluting abundant spins by isotope edited radio frequency field assisted diffusion. J. Am. Chem. Soc 2004, 126, 7196–7197. [PubMed: 15186155]
34. Huster D; Yao XL; Hong M, Membrane protein topology probed by H-1 spin diffusion from lipids using solid-state NMR spectroscopy. J. Am. Chem. Soc 2002, 124 (5), 874–883. [PubMed: 11817963]
35. Kumashiro KK; Schmidt-Rohr K; Murphy OJ; Ouellette KL; Cramer WA; Thompson LK, A novel tool for probing membrane protein structure: solid-state NMR with proton spin diffusion and X-nucleus detection. J. Am. Chem. Soc 1998, 120, 5043–5051.
36. Schmidt-Rohr K; Spiess HW Multidimensional Solid-State NMR and Polymers; 1st ed.; Academic Press: San Diego, 1994; p 478.
37. Wang T; Jo H; DeGrado WF; Hong M, Water Distribution, Dynamics, and Interactions with Alzheimer's β-Amyloid Fibrils Investigated by Solid-State NMR. J. Am. Chem. Soc 2017, 139, 6242–6252. [PubMed: 28406028]
38. Liao SY; Fritzsching KJ; Hong M, Conformational analysis of the full-length M2 protein of the influenza A virus using solid-state NMR. Protein Sci 2013, 22 (11), 1623–1638. [PubMed: 24023039]
39. Ader C; Schneider R; Seidel K; Etzkorn M; Becker S; Baldus M, Structural rearrangements of membrane proteins probed by water-edited solid-state NMR spectroscopy. J. Am. Chem. Soc 2009, 131, 170–176. [PubMed: 19063626]
40. Jaroniec CP; Tounge BA; Herzfeld J; Griffin RG, Frequency selective heteronuclear dipolar recoupling in rotating solids: Accurate C-13-N-15 distance measurements in uniformly C-13,N-15-labeled peptides. J. Am. Chem. Soc 2001, 123 (15), 3507–3519. [PubMed: 11472123]

41. deAzevedo ER; Hu WG; Bonagamba TJ; Schmidt-Rohr K, Centerband-only detection of exchange: Efficient analysis of dynamics in solids by NMR. J. Am. Chem. Soc 1999, 121 (36), 8411–8412.
42. Luo W; Hong M, Determination of the oligomeric number and intermolecular distances of membrane protein assemblies by anisotropic ^{1}H-driven spin diffusion NMR spectroscopy. J. Am. Chem. Soc 2006, 128 (22), 7242–7251. [PubMed: 16734478]
43. Buffy JJ; Waring AJ; Lehrer RI; Hong M, Immobilization and Aggregation of Antimicrobial Peptide Protegrin in Lipid Bilayers Investigated by Solid-State NMR. Biochemistry-Us 2003, 42, 13725–13734.
44. Huster D; Xiao LS; Hong M, Solid-state NMR investigation of the dynamics of the soluble and membrane-bound colicin Ia channel-forming domain. Biochemistry-Us 2001, 40 (25), 7662–7674.
45. Tang M; Waring AJ; Hong M, Arginine dynamics in a membrane-bound cationic beta-hairpin peptide from solid-state NMR. Chembiochem 2008, 9 (9), 1487–1492. [PubMed: 18442147]
46. Su Y; Doherty T; Waring AJ; Ruchala P; Hong M, Roles of arginine and lysine residues in the translocation of a cell-penetrating peptide from (13)C, (31)P, and (19)F solid-state NMR. Biochemistry-Us 2009, 48, 4587–4595.
47. Bielecki A; Kolbert AC; Levitt MH, Frequency-Switched Pulse Sequences: Homonuclear Decoupling and Dilute Spin NNM in Solids. Chem. Phys. Lett 1989, 155 (4-5), 341–346.
48. Hohwy M; Rienstra CM; Jaroniec CP; Griffin RG, Fivefold symmetric homonuclear dipolar recoupling in rotating solids: Application to double quantum spectroscopy. J. Chem. Phys 1999, 110 (16), 7983–7992.
49. Mani R; Buffy JJ; Waring AJ; Lehrer RI; Hong M, Solid-State NMR Investigation of the Selective Disruption of Lipid Membranes by Protegrin-1. Biochemistry-Us 2004, 43, 13839–13848.
50. Mani R; Waring AJ; Lehrer RI; Hong M, Membrane-disruptive abilities of beta-hairpin antimicrobial peptides correlate with conformation and activity: a 31P and 1H NMR study. Biochim. Biophys. Acta 2005, 1716, 11–18. [PubMed: 16182236]
51. Yamaguchi S; Waring A; Hong T; Lehrer R; Hong M Solid-State NMR Investigations of Peptide-Lipid Interaction and Orientation of a beta-Sheet Antimicrobial Peptide, Protegrin. Biochemistry-Us 2002, 41, 9852–9862.
52. Doherty T; Hong M, 2D H-1-P-31 solid-state NMR studies of the dependence of interbilayer water dynamics on lipid headgroup structure and membrane peptides. J. Magn. Reson 2009, 196 (1), 39–47. [PubMed: 18938095]
53. Yao H; Hong M, Membrane-dependent conformation, dynamics, and lipid interactions of the fusion peptide of the paramyxovirus PIV5 from solid-state NMR. J. Mol. Biol 2013, 425, 563–576. [PubMed: 23183373]
54. Yao H; Hong M, Conformation and Lipid Interaction of the Fusion Peptide of the Paramyxovirus PIV5 in Anionic and Negative-Curvature Membranes From Solid-State NMR. J. Am. Chem. Soc 2014, 136, 2611–2624. [PubMed: 24428385]
55. Yao H; Lee MW; Waring AJ; Wong GC; Hong M, Viral fusion protein transmembrane domain adopts beta-strand structure to facilitate membrane topological changes for virus-cell fusion. Proc. Natl. Acad. Sci. USA 2015, 112 (35), 10926–10931. [PubMed: 26283363]
56. Bak M; Rasmussen JT; Nielsen NC, SIMPSON: A general simulation program for solid-state NMR spectroscopy. J. Magn. Reson 2000, 147 (2), 296–330. [PubMed: 11097821]
57. Sinha N; Schmidt-Rohr K; Hong M, Compensation for Pulse Imperfections in Rotational-Echo Double-Resonance NMR by Composite Pulses and EXORCYCLE. J. Magn. Reson 2004, 168, 358–365. [PubMed: 15140448]
58. Jo S; Kim T; Iyer VG; Im W, CHARMM-GUI: a web-based graphical user interface for CHARMM. J. Comput. Chem 2008, 29 (11), 1859–1865. [PubMed: 18351591]
59. Pronk S; Pall S; Schulz R; Larsson P; Bjelkmar P; Apostolov R; Shirts MR; Smith JC; Kasson PM; van der Spoel D; Hess B; Lindahl E, GROMACS 4.5: a high-throughput and highly parallel open source molecular simulation toolkit. Bioinformatics 2013, 29 (7), 845–854. [PubMed: 23407358]
60. Yang Y; Yao H; Hong M, Distinguishing Bicontinuous Lipid Cubic Phases from Isotropic Membrane Morphologies Using 31P Solid-State NMR Spectroscopy. J. Phys. Chem 2015, 119, 4993–5001.

61. Schmidt N; Mishra A; Lai GH; Wong GC, Arginine-rich cell-penetrating peptides. FEBS Lett 2010, 584, 1806–1813. [PubMed: 19925791]

62. Schmidt NW; Mishra A; Wang J; DeGrado WF; Wong GC, Influenza virus A M2 protein generates negative Gaussian membrane curvature necessary for budding and scission. J. Am. Chem. Soc 2013, 135, 13710–13719. [PubMed: 23962302]

63. Saffman PG; Delbruck M, Brownian motion in biological membranes. Proc. Natl. Acad. Sci. USA 1975, 72 (8), 3111–3113. [PubMed: 1059096]

64. Cady SD; Goodman C; Tatko C; DeGrado WF; Hong M, Determining the orientation of uniaxially rotating membrane proteins using unoriented samples: a 2H, 13C, and 15N solid-state NMR investigation of the dynamics and orientation of a transmembrane helical bundle. J. Am. Chem. Soc 2007, 129, 5719–5729. [PubMed: 17417850]

65. Cady SD; Hong M, Simultaneous extraction of multiple orientational constraints of membrane proteins by 13C-detected N-H dipolar couplings under magic angle spinning. J. Magn. Reson 2008, 191, 219–225. [PubMed: 18221902]

66. Aisenbrey C; Bechinger B, Investigations of polypeptide rotational diffusion in aligned membranes by 2H and 15N solid-state NMR spectroscopy. J. Am. Chem. Soc 2004, 126, 16676–16683. [PubMed: 15600374]

67. Mani R; Cady SD; Tang M; Waring AJ; Lehrer RI; Hong M, Membrane-dependent oligomeric structure and pore formation of a beta-hairpin antimicrobial peptide in lipid bilayers from solid-state NMR. Proc. Natl. Acad. Sci. USA 2006, 103, 16242–16247. [PubMed: 17060626]

68. Elkins MR; Williams JK; Gelenter MD; Dai P; Kwon B; Sergeyev IV; Pentelute BL; Hong M, Cholesterol-binding site of the influenza M2 protein in lipid bilayers from solid-state NMR. Proc. Natl. Acad. Sci. U. S. A 2017, 114, 12946–12951. [PubMed: 29158386]

69. Shcherbakov AA; Hong M, Rapid Measurement of Long-Range Distances in Proteins by Multidimensional 13C-19F REDOR NMR under Fast Magic-Angle Spinning. J. Biomol. NMR 2018, in press.

70. Lovell SC; Word JM; Richardson JS; Richardson DC, The penultimate rotamer library. Proteins 2000, 40, (3), 389–408. [PubMed: 10861930]

71. Yin HS; Wen X; Paterson RG; Lamb RA; Jardetzky TS, Structure of the parainfluenza virus 5 F protein in its metastable, prefusion conformation. Nature 2006, 439, 38–44. [PubMed: 16397490]

72. Yin HS; Paterson RG; Wen X; Lamb RA; Jardetzky TS, Structure of the uncleaved ectodomain of the paramyxovirus (hPIV3) fusion protein. Proc. Natl. Acad. Sci. U. S. A 2005, 102 (26), 9288–9293. [PubMed: 15964978]

73. Hong M; Doherty T, Orientation determination of membrane-disruptive proteins using powder samples and rotational diffusion: a simple solid-state NMR approach. Chem. Phys. Lett 2006, 432, 296–300. [PubMed: 17364006]

74. Su Y; Li S; Hong M, Cationic membrane peptides: atomic-level insight of structureactivity relationships from solid-state NMR. Amino Acids 2013, 44, 821–833. [PubMed: 23108593]

75. Su Y; DeGrado WF; Hong M, Orientation, dynamics, and lipid interaction of an antimicrobial arylamide investigated by 19F and 31P solid-state NMR spectroscopy. J. Am. Chem. Soc 2010, 132, 9197–9205. [PubMed: 20536141]

76. de Jesus AJ; Allen TW, The role of tryptophan side chains in membrane protein anchoring and hydrophobic mismatch. Biochim. Biophys. Acta 2013, 1828, 864–876. [PubMed: 22989724]

77. Killian JA; von Heijne G, How proteins adapt to a membrane-water interface. Trends Biochem. Sci 2000, 25, 429–434. [PubMed: 10973056]

78. Traaseth NJ; Verardi R; Torgersen KD; Karim CB; Thomas DD; Veglia G, Spectroscopic validation of the pentameric structure of phospholamban. Proc. Natl. Acad. Sci. U. S. A 2007, 104, 14676–14681. [PubMed: 17804809]

79. Verardi R; Shi L; Traaseth NJ; Walsh N; Veglia G, Structural topology of phospholamban pentamer in lipid bilayers by a hybrid solution and solid-state NMR method. Proc. Natl. Acad. Sci. U. S. A 2011, 108, 9101–9106. [PubMed: 21576492]

80. Donald JE; Zhang Y; Fiorin G; Carnevale V; Slochower DR; Gai F; Klein ML; DeGrado WF, Transmembrane orientation and possible role of the fusogenic peptide from parainfluenza virus 5

(PIV5) in promoting fusion. Proc. Natl. Acad. Sci. U. S. A 2011, 108, 3958–3963. [PubMed: 21321234]

81. Bissonnette ML; Donald JE; DeGrado WF; Jardetzky TS; Lamb RA, Functional analysis of the transmembrane domain in paramyxovirus F protein-mediated membrane fusion. J. Mol. Biol 2009, 386, 14–36. [PubMed: 19121325]
82. Ollesch J; Poschner BC; Nikolaus J; Hofmann MW; Herrmann A; Gerwert K; Langosch D, Secondary structure and distribution of fusogenic LV-peptides in lipid membranes. Eur. Biophys. J 2008, 37 (4), 435–445. [PubMed: 18038229]
83. Poschner BC; Quint S; Hofmann MW; Langosch D, Sequence-Specific Conformational Dynamics of Model Transmembrane Domains Determines Their Membrane Fusogenic Function. J. Mol. Biol 2009, 386 (3), 733–741. [PubMed: 19154744]
84. Poschner BC; Fischer K; Herrmann JR; Hofmann MW; Langosch D, Structural features of fusogenic model transmembrane domains that differentially regulate inner and outer leaflet mixing in membrane fusion. Mol. Membr. Biol 2010, 27 (1), 1–10. [PubMed: 19939203]
85. Yao H; Lee M; Liao SY; Hong M, Solid-State Nuclear Magnetic Resonance Investigation of the Structural Topology and Lipid Interactions of a Viral Fusion Protein Chimera Containing the Fusion Peptide and Transmembrane Domain. Biochemistry-Us 2016, 55, 6787–6800.
86. Qiang W; Sun Y; Weliky DP, A strong correlation between fusogenicity and membrane insertion depth of the HIV fusion peptide. Proc. Natl. Acad. Sci. U. S. A 2009, 106 (36), 15314–15319. [PubMed: 19706388]
87. Yang J; Gabrys CM; Weliky DP, Solid-state nuclear magnetic resonance evidence for an extended beta strand conformation of the membrane-bound HIV-1 fusion peptide. Biochemistry-Us 2001, 40 (27), 8126–8137.
88. Apellaniz B; Rujas E; Carravilla P; Requejo-Isidro J; Huarte N; Domene C; Nieva JL, Cholesterol-dependent membrane fusion induced by the gp41 membrane-proximal external region-transmembrane domain connection suggests a mechanism for broad HIV-1 neutralization. J. Virol. 2014, 88 (22), 13367–13377. [PubMed: 25210180]
89. Irimia A; Serra AM; Sarkar A; Jacak R; Kalyuzhniy O; Sok D; Saye-Francisco KL; Schiffner T; Tingle R; Kubitz M; Adachi Y; Stanfield RL; Deller MC; Burton DR; Schief WR; Wilson IA, Lipid interactions and angle of approach to the HIV-1 viral membrane of broadly neutralizing antibody 10E8: Insights for vaccine and therapeutic design. PLoS Pathog 2017, 13 (2), e1006212. [PubMed: 28225819]
90. Reuven EM; Dadon Y; Viard M; Manukovsky N; Blumenthal R; Shai Y, HIV-1 gp41 Transmembrane Domain Interacts with the Fusion Peptide: Implication in Lipid Mixing and Inhibition of Virus-Cell Fusion. Biochemistry-Us 2012, 51 (13), 2867–2878.

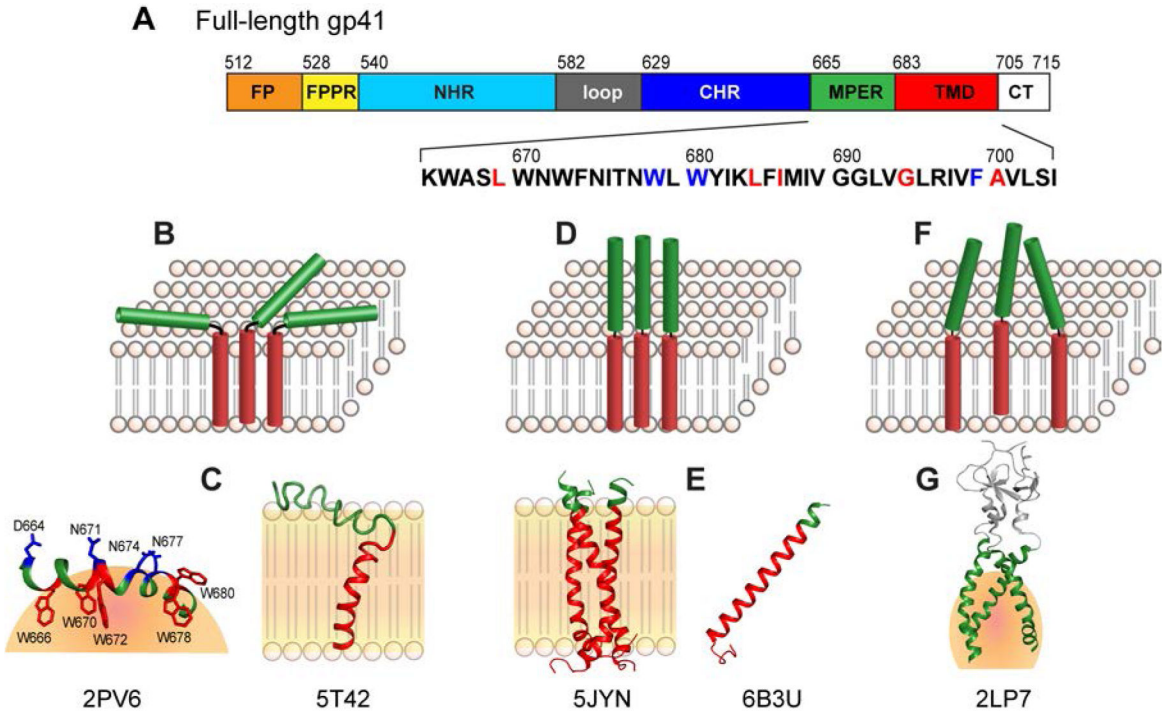

Figure 1.

Amino acid sequence (**A**) and structural models (**B-G**) of the gp41 MPER-TMD. (**A**) Domains in gp41. The MPER-TMD peptide used in this study spans residues K665 to I704. Fluorinated residues are highlighted in blue while ^{13}C, ^{15}N-labeled residues are shown in red. (**B**) Schematic of the helix-turn-helix model. (**C**) Structures of the gp41 MPER peptide (PDB code: 2PV6) and Ebola GP2 MPER-TMD peptide (PDB code: 5T42) that support the helix-turn-helix model. (**D**) Schematic of the continuous helix model. (**E**) Structures of gp41 (677-716) that support the continuous-helix model. One structure is a trimer (PDB code: 5JYN) while the other is a tilted monomer (PDB code: 6B3U). (**F**) Schematic of the trimeric MPER and monomeric TMD model. (**G**) Structure of an engineered MPER trimer (PDB code: 2LP7) that supports this model.

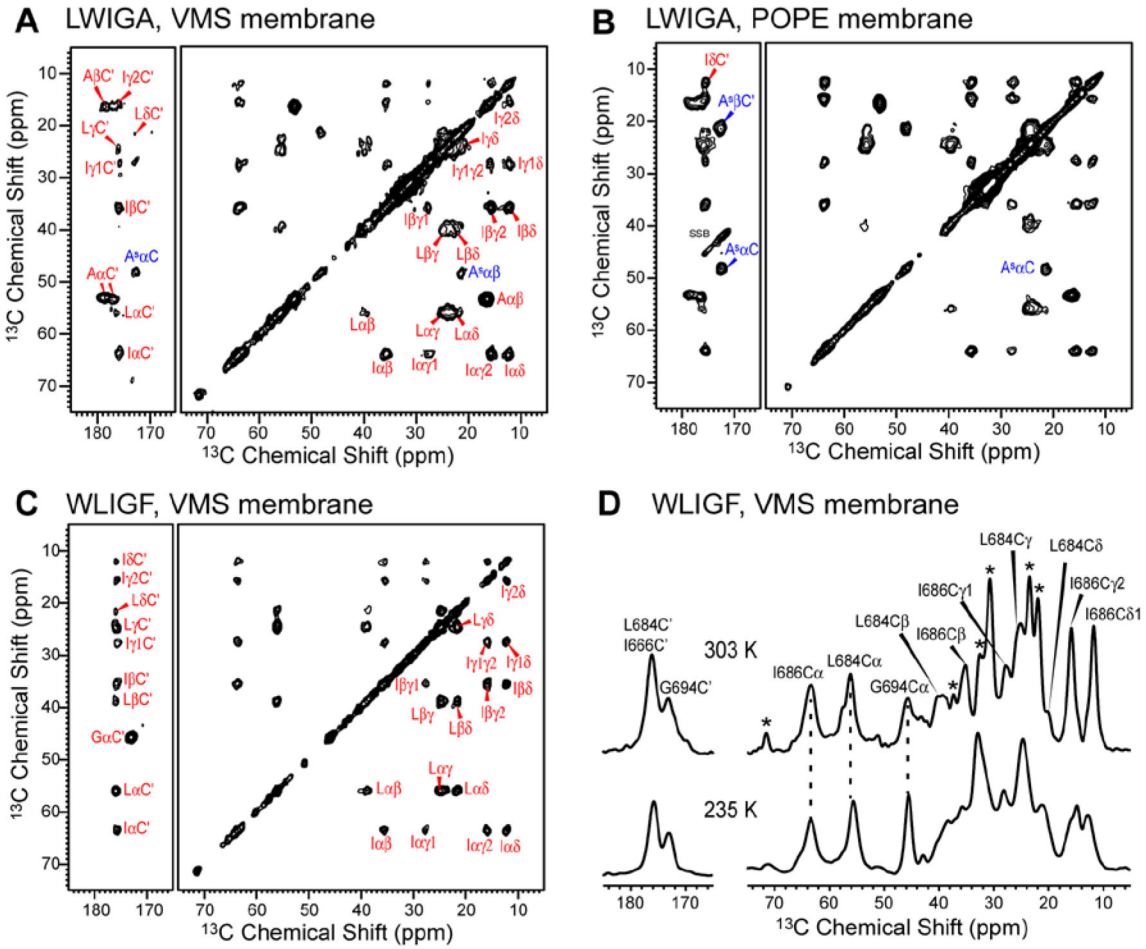

Figure 2.

2D ^{13}C-^{13}C correlation spectra of ^{13}C, ^{15}N-labeled MPER-TMD in VMS and POPE membranes, measured at 263 K with a ^{13}C mixing time of 100 ms. (**A**) VMS-bound LWIGA peptide. Most residues show α-helical chemical shifts, except for A700, which exhibits a second Cα-Cβ cross peak at β-strand chemical shifts. (**B**) POPE-bound LWIGA peptide, showing similar chemical shifts as the VMS-bound peptide. (**C**) VMS-bound WLIGF peptide, showing purely α-helical chemical shifts. (**D**) 1D ^{13}C spectra of VMS-bound WLIGF peptide at 303 K and 235 K. The chemical shifts are unchanged, indicating that the MPER-TMD structure is the same at low and high temperatures.

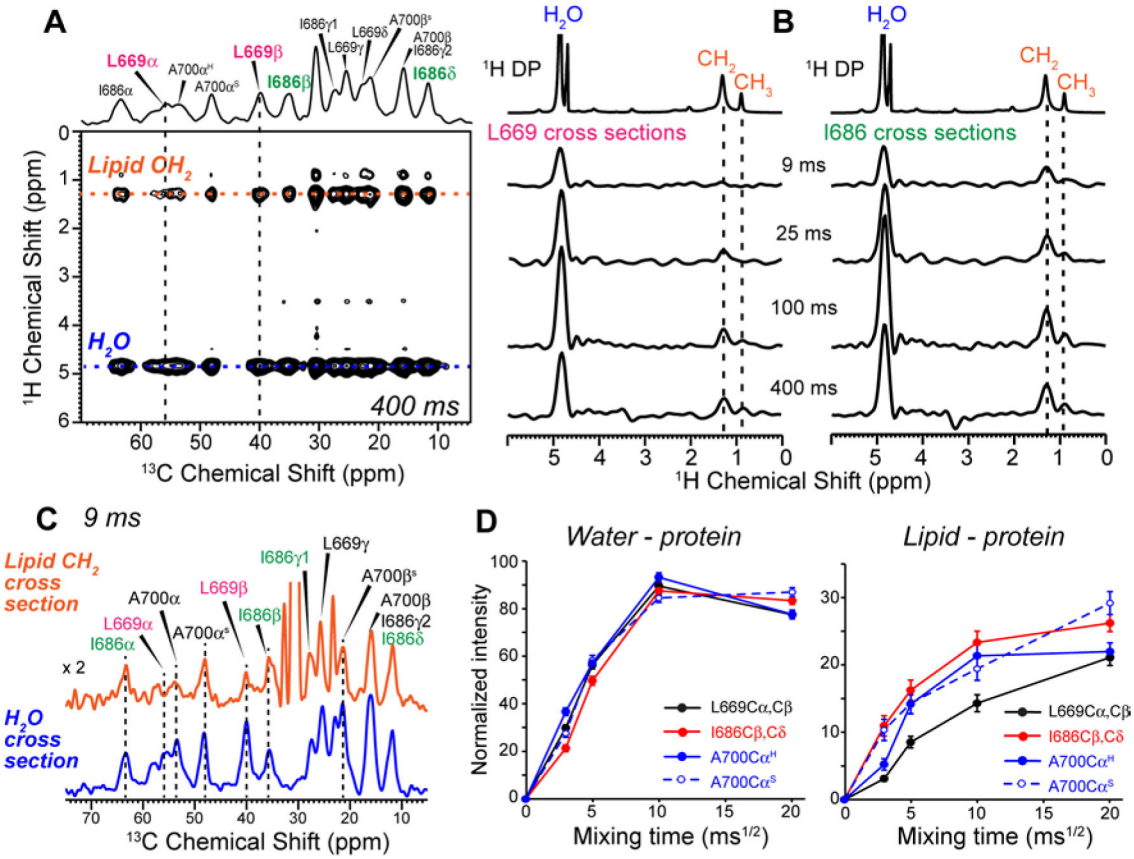

Figure 3.

Depths of insertion of gp41 MPER-TMD in the POPE membrane, measured at 303 K. (**A**) 2D ^{1}H-^{13}C correlation spectrum of LWIGA, measured with 400 ms ^{1}H spin diffusion. (**B**) ^{1}H cross sections of L669 and I686 as a function of mixing time. The lipid cross peaks of L669 are weaker than the lipid cross peaks of I686, indicating that L669 lies on the membrane surface while I686 is embedded in the membrane. (**C**) ^{13}C cross sections at the lipid CH_2 and water ^{1}H chemical shifts, extracted from the 9 ms 2D spectrum. L669 has higher water cross peaks and lower lipid cross peaks compared to other residues, indicating that it lies on the membrane surface. (**D**) Water-to-protein and lipid-to-protein ^{1}H polarization transfer curves as a function of mixing time. Residue I686 has the fastest transfer from lipids and the slowest transfer from water, while the opposite is observed for L669.

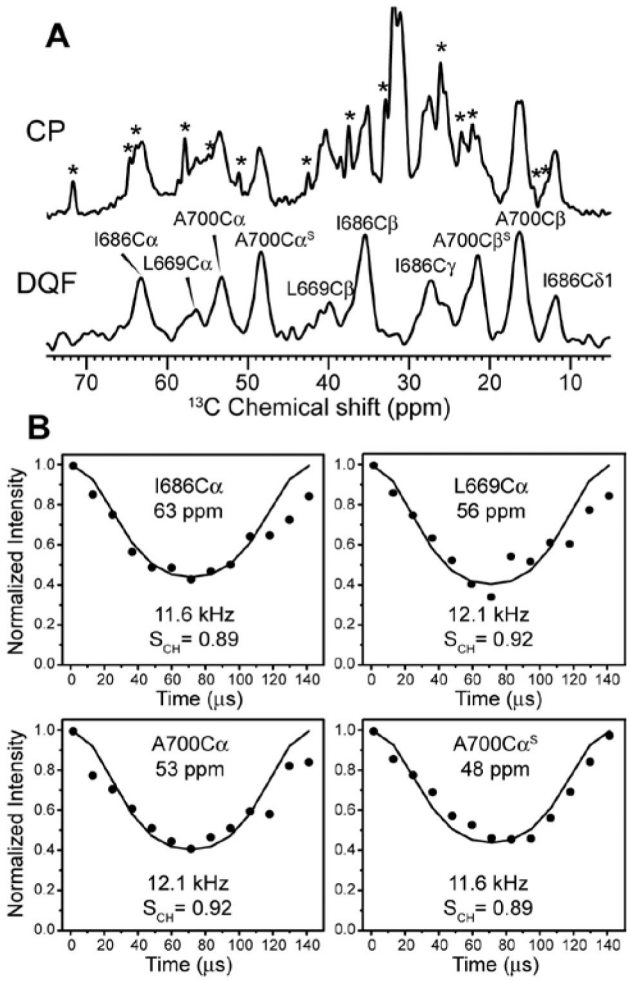

Figure 4.

(**A**) 1D ^{13}C CP and double-quantum filtered (DQF) spectra of VMS-bound LWIGA peptide at 303 K. Asterisks in the CP spectrum indicate lipid peaks, which are suppressed in the DQF spectrum. (**B**) ^{13}C-^{1}H dipolar couplings curves of VMS-bound LWIGA peptide, extracted from a 2D DQF-DIPSHIFT spectrum. Backbone Cα-Hα order parameters are 0.89-0.92, indicating that the peptide is mostly immobilized in the VMS membrane at 303 K.

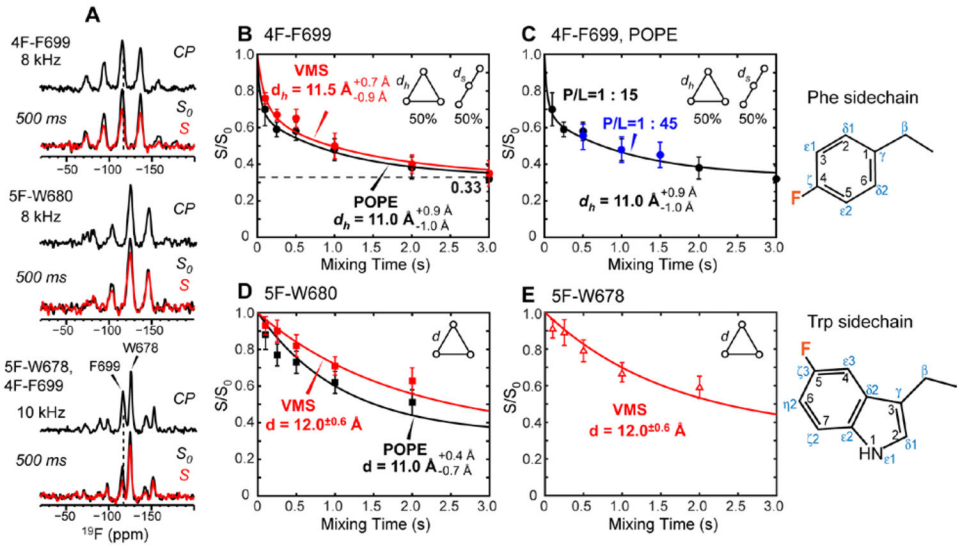

Figure 5.

^{19}F CODEX data to determine the oligomeric state and interhelical distances of MPER-TMD in lipid membranes. (**A**) Representative ^{19}F cross polarization (CP) and CODEX S_0 and S spectra of the three fluorinated residues in the VMS membrane. (**B**) 4F-F699 CODEX data, showing an equilibrium echo intensity of ~0.33 in both VMS and POPE membranes, proving that the peptide is trimerized. (**C**) ^{19}F CODEX data of 4F-F699 at P/L ratios of 1 : 15 (black) and 1 : 45 (blue) in POPE membranes. Similar dephasing is observed at both peptide concentrations. (**D**) W680 ^{19}F CODEX data, showing single-exponential decays, which are best fit to nearest-neighbor distances of 11.0 Å for the POPE sample and 12.0 Å for the VMS sample. (**E**) 5F-W678 CODEX data of VMS-bound peptide, showing an interhelical distance of 12.0 Å. Distance uncertainties are indicated in the panels. The chemical structures of 4F-Phe and 5F-Trp sidechains are shown on the right, where the sidechain numbering and IUPAC nomenclatures are both indicated.

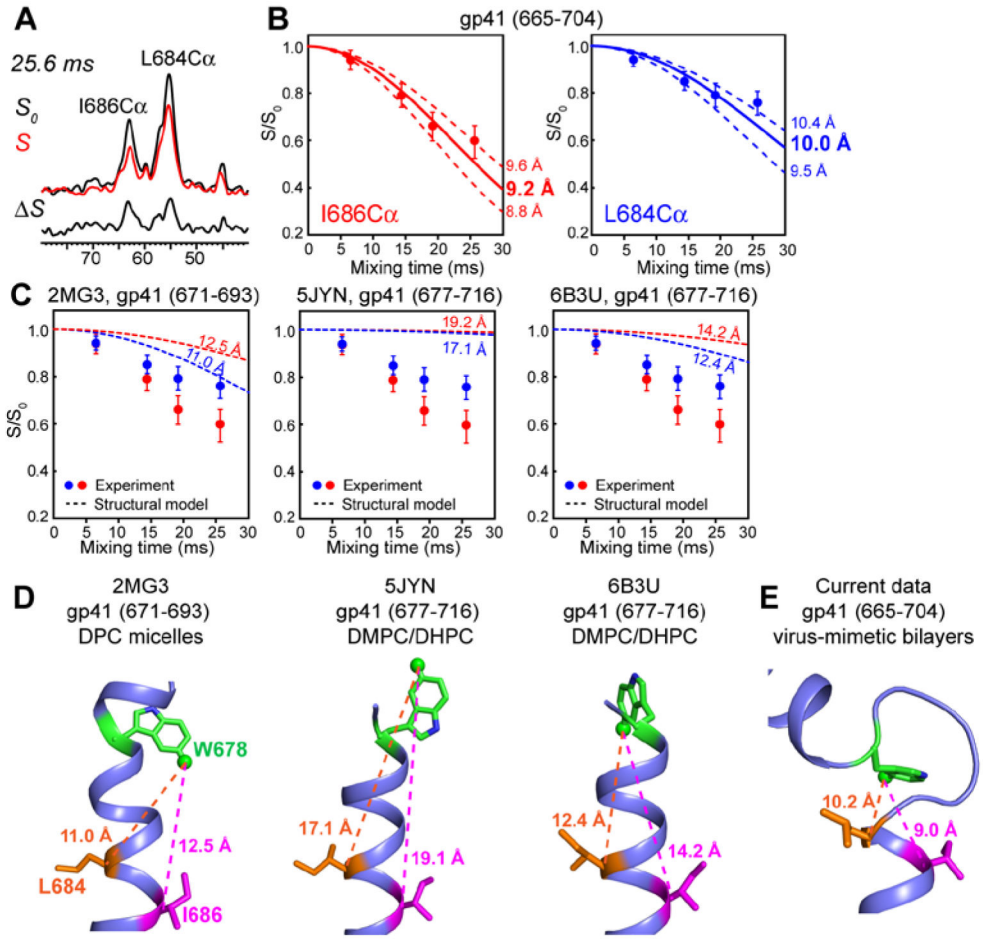

Figure 6.

^{13}C-^{19}F REDOR data of WLIGF-labeled MPER-TMD in the VMS membrane, measured at 235 K. (**A**) Representative ^{13}C spectra measured without (S_0) and with (S) ^{19}F pulses. 5F-W678 caused significant dipolar dephasing to I686 and L684 Cα. (**B**) ^{13}C-^{19}F REDOR curves for I686Cα and L684Cα. The data are best fit to distances of 9.2 Å for I686 Cα and 10.0 Å for L684 Cα. (**C**) Comparison of the measured REDOR data (symbols) with the predicted ^{13}C-^{19}F REDOR curves (dashed lines) for three structural models of gp41 (**D**), which show 5F-W678 to L684 and I686 Cα distances that are much longer than the measured values. (**E**) Proposed turn structure between the MPER and TMD, constrained by the measured ^{13}C-^{19}F and ^{19}F-^{19}F distances.

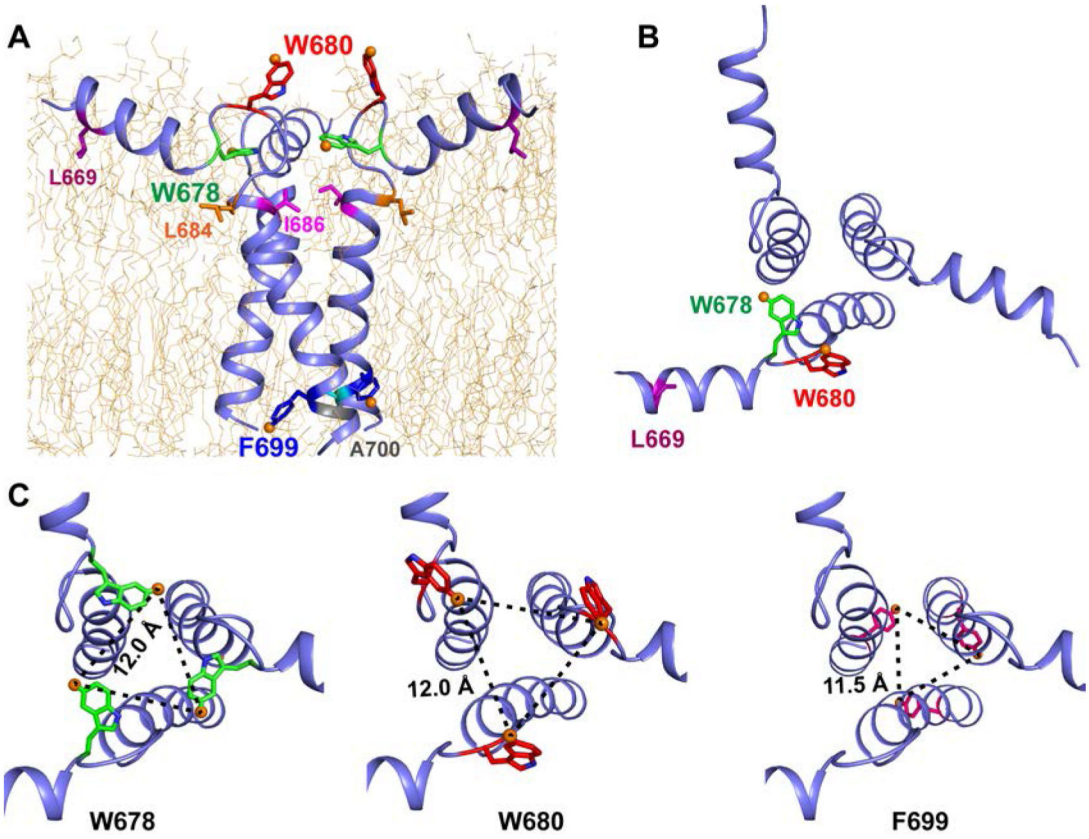

Figure 7.

Structure topology and trimer association of gp41 MPER-TMD in virus-mimetic membranes, obtained from MD simulations using template-E alignment, the measured distance constraints and the TMD (ϕ ψ) angles from the PDB structure 5JYN. (**A**) Side view, showing the MPER on the membrane surface and the TMD spanning the bilayer. (**B**) Top view of the locations of W680, W678, and L669 in the MPER. The exact structure of the turn is not fully determined by the data shown here, thus this structural model should be considered one of the possible structures. (**C**) Top view of the trimeric MPER-TMD, showing the rotameric structures and interhelical distances of W678, W680, and F699.

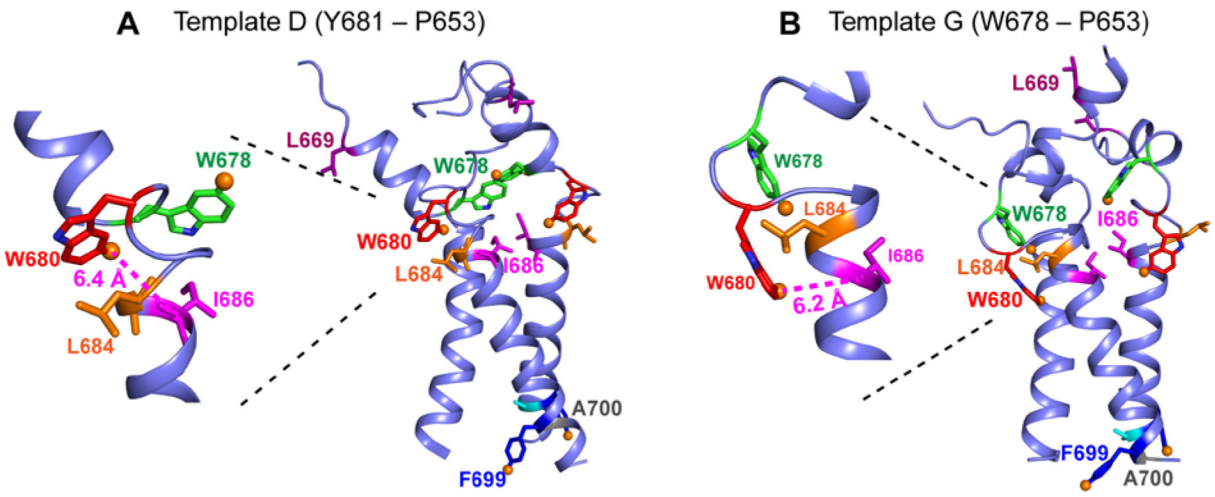

Figure 8.

Alternative structural models of the MPER-TMD that are inconsistent with the data. (**A**) Structural model based on template D, where Y681 of gp41 is aligned with P653 of the Ebola fusion protein. The TMD (ϕ, ψ) torsion angles were taken from PDB structure 6B3U. 5F-W680 is 6.4 Å from I686Cα, which is inconsistent with the ^{13}C-^{19}F REDOR data. (**B**) Structural model based on template G, where W678 of gp41 is aligned with P653 of the Ebola fusion protein. L669 of the MPER faces solution and 5F-W680 is 6.2 Å from I686Cα, both of which are inconsistent with the experimental data.

Table 1.

Amino acid sequence of the HXB2 HIV-1 gp41 peptide (residues 665-704) used in this study. This sequence is compared with the clade D gp41 TMD-CT peptide (residues 677-716) studied by solution NMR.

665	670	680	690	700	710
KWASL	WNWFNITNWL	WYIKLFIMIV	GGLVGLRIVF	AVLSI	
	NWL	WYIRIFIIIV	GSLIGLRIVF	AVLSLVNRVR	QGYSPLS

Table 2.

gp41 MPER-TMD membrane samples prepared in this work.

Isotopically labeled peptide	Lipid membrane
F699: 4-^{19}F-F699	POPE VMS
LWIGA: U-^{13}C, ^{15}N-L669, I686, A700, ^{13}C'-G694, 5-^{19}F-W680	VMS POPE
WLIGF: U-^{13}C, ^{15}N-L684, I686, G694, 5-^{19}F-W678, 4-^{19}F-F699	VMS

Table 3.

Experimentally measured ^{13}C-^{19}F and ^{19}F-^{19}F distances for VMS membrane-bound gp41 MPER-TMD.

	Residues	Measured distances
Intramolecular	5F-W678 to L684Cα	$10.0^{\pm 0.5}$ Å
	5F-W678 to I686Cα	$9.2^{\pm 0.4}$ Å
	5F-W678 to 5F W678	$12.0^{\pm 0.6}$ Å
Intermolecular	5F-W680 to 5F-W680	$12.0^{\pm 0.6}$ Å
	4F-F699 to 4F-F699	$11.0^{\pm 1.0}$ Å